

# Implications of 98 GeV and 125 GeV Higgs scenario in non-decoupling SUSY with updated ATLAS, CMS and PLANCK data

Biplob Bhattacharjee<sup>a1</sup>, Manimala Chakraborti<sup>b2</sup>, Amit Chakraborty<sup>b3</sup>, Utpal Chattopadhyay<sup>b4</sup>, Debottam Das<sup>c5</sup>, and Dilip Kumar Ghosh<sup>b6</sup>

<sup>a</sup> Kavli Institute for the Physics and Mathematics of the Universe (WPI),  
The University of Tokyo, Kashiwa, Chiba 277-8583, Japan

<sup>b</sup> Department of Theoretical Physics, Indian Association for the Cultivation of Science,  
2A & B Raja S.C. Mullick Road, Jadavpur, Kolkata 700 032, India

<sup>c</sup> Institut für Theoretische Physik und Astrophysik, Universität Würzburg,  
Am Hubland, 97074 Würzburg, Germany

## Abstract

We discuss both MSSM and NMSSM scenarios in which the lightest Higgs boson with  $m_h = 98$  GeV is consistent with the small excess ( $\sim 2.3\sigma$ ) observed at the LEP in  $e^+e^- \rightarrow Zh$ , with  $h \rightarrow b\bar{b}$  process and the heavier Higgs boson of mass close to 125 GeV as the observed candidate of the SM Higgs like particle at the LHC. We show the allowed regions in the non-decoupling Higgs zone of MSSM parameter space which are consistent with several low energy constraints coming from heavy flavour physics, latest experimental data on Higgs signals and lower limit on superparticle masses from 7 TeV and 8 TeV LHC run. We also implement the constraints from the relic density of the cold dark matter as obtained from the recent PLANCK data. Additionally, we discuss the possibility of observing the light Higgs boson of mass 98 GeV at the 14 TeV LHC run via  $pp \rightarrow Vh$ , with  $h \rightarrow b\bar{b}$  using the technique of jet substructure. Our analysis shows that at 14 TeV LHC run with  $300 \text{ fb}^{-1}$  luminosity the signal efficiency of such a light Higgs boson is at most  $2.5\sigma$ . Finally, we make a comment on the prospect of proposed  $e^+e^-$  ILC to discover/exclude this light Higgs boson.

## 1 Introduction

The Large Hadron Collider (LHC) announcements on discovery of the Higgs boson ( $\hat{h}$ ) like particle as analyzed by the CMS [1] and ATLAS [2] collaborations have been highly encouraging for particle physicists who had been in search of the Higgs boson through several decades. Additionally, CDF

<sup>1</sup>biplob.bhattacharjee@ipmu.jp, <sup>2</sup>tpmc@iacs.res.in, <sup>3</sup>tpac@iacs.res.in, <sup>4</sup>tpuc@iacs.res.in, <sup>5</sup>debottam.das@physik.uni-wuerzburg.de, <sup>6</sup>tpdkg@iacs.res.in

and D0 experiments of the Tevatron at Fermilab also announced a result on  $h \rightarrow b\bar{b}$  where Higgs boson is produced in the associated vector boson mode  $W h / Z h$  [3]. Within the Standard Model (SM) [4] one can compute Higgs production cross sections via different means as well as consider decay of Higgs to various final products [5]. For the production mode, the main contributing sources are (i) gluon-gluon fusion (ggF), (ii) vector boson fusion (VBF) and (iii) associated production with vector bosons ( $Vh$ ), where V generically stands for W and Z-bosons. The decay channels which are directly concerned with detection and prediction of Higgs mass, are  $ZZ^*$ ,  $WW^*$ ,  $b\bar{b}$ ,  $\gamma\gamma$ ,  $\tau^+\tau^-$  etc. Here  $V^*$  refers to off-shell vector boson indicating  $h \rightarrow VV^* \rightarrow V f \bar{f}$ . The two photon ( $\gamma\gamma$ ) final state refers to loop induced processes involving W-boson and heavy fermions like  $t, b$ -quarks and  $\tau$ -lepton in the loop. The dominance of a heavier fermion rather than a lighter one is of course due to larger  $h f \bar{f}$  coupling. The recent LHC observations of Higgs are associated with the following channels:  $\gamma\gamma$ ,  $ZZ^*$  ( $\rightarrow 4l$ ),  $WW^*$  ( $\rightarrow l\nu l\nu$ , or  $\rightarrow l\nu jj$ ). LHC observations in the di-photon and the 4-lepton decay channels indeed lead to the discovery of Higgs boson with mass  $\sim 125$  GeV at around  $5\sigma$  level [6, 7]. The ongoing Higgs search at LHC is very important because it may successfully probe the origins of electroweak symmetry breaking and it may also provide valuable information for scenarios Beyond the Standard Model (BSM) of particle physics. Undoubtedly, low energy supersymmetry (SUSY) has been a promising direction to travel in order to look for BSM effects in particle physics. The modest  $N = 1$  supersymmetric extension of SM, namely the Minimal Supersymmetric Standard Model (MSSM) [8] has two Higgs doublets and this leads to several Higgs scalars. The MSSM Higgs states are: two CP-even neutral Higgs scalar bosons  $h$  and  $H$ , one CP-odd neutral Higgs scalar boson  $A$ , and two charged Higgs scalar bosons  $H^\pm$  [8, 9]. Although MSSM has a large number of parameters, the Higgs sector, while not considering any radiative corrections can be described by only a few parameters. Apart from the experimentally determined mass of Z-boson  $M_Z$ , these are: i)  $M_A$ , the pseudoscalar Higgs mass parameter and ii)  $\tan\beta$ , the ratio of the Higgs vacuum expectation values  $\langle H_2 \rangle / \langle H_1 \rangle$ , where  $H_1$  and  $H_2$  give masses to down type of quarks and leptons and up type of quarks respectively. However, there can be a significant amount of radiative corrections to the masses of the Higgs bosons and this causes a few other MSSM parameters to be relevant like the parameters that are involved in top squark and to some extent bottom squark or even tau-slepton masses [9, 10]. MSSM has a nice prediction of a 135 GeV upper limit for the mass  $m_h$  of the lightest Higgs boson [11]. Finding the observed Higgs boson to have a mass in the vicinity of 125 GeV at LHC is very exciting for pursuing SUSY as a scenario beyond the SM.

The MSSM Higgs sector can be broadly divided into a decoupling and a non-decoupling zone [9]. The former region corresponds to pseudoscalar mass  $M_A$  becoming very large (in practice above 300

GeV or so). In this limit,  $\cos^2(\beta - \alpha)$  becomes vanishingly small (consequently  $\sin^2(\beta - \alpha) \rightarrow 1$ ). Here,  $\alpha$  refers to the Higgs mixing angle. The couplings like  $W^+W^-H$ ,  $HZZ$ ,  $ZAh$ ,  $W^\pm H^\mp h$ ,  $ZW^\pm H^\mp h$ ,  $\gamma W^\pm H^\mp h$  are all proportional to  $\cos(\beta - \alpha)$ . On the other hand,  $W^+W^-h$ ,  $hZZ$ ,  $ZAH$ ,  $W^\mp H^\pm H$ ,  $ZW^\mp H^\pm H$  and  $\gamma W^\mp H^\pm H$  couplings are all proportional to  $\sin(\beta - \alpha)$ . In the decoupling limit, an obvious possibility is to interpret the newly observed state at around 125 GeV as the light  $CP$ -even Higgs boson having SM-like couplings (for details see Refs. [12–14]). As a consequence, all other Higgs bosons become much heavier than  $h$ . The non-decoupling region on the other hand is specified by  $M_h \sim M_A \sim M_H \sim M_Z$  or  $\sin^2(\beta - \alpha)$  becoming very small. In the LHC context, the non-decoupling region with  $\cos^2(\beta - \alpha)$  becoming close to unity would mean larger coupling strength of  $H$  with the electroweak gauge bosons. Thus here we may explore the possibility of  $m_H \sim 125$  GeV, instead of considering the lighter counterpart  $h$  to correspond to the discovered boson. Here the heavier Higgs field  $H$  would have SM-like couplings whereas the lighter Higgs  $h$  would have much weaker couplings to  $W$  and  $Z$ -bosons, for details see Ref. [15–18].

We further consider  $m_h$  to be in the vicinity of 98 GeV in the light of an old result from LEP Collaborations in regard to  $e^+e^- \rightarrow Z\tilde{h}$  with  $\tilde{h} \rightarrow b\bar{b}$  where the result indicated a possibility of seeing an excess of Higgs-like events [19] near the above value of mass. This excess came with a significance level of 2.3 times the standard deviations in the combined analysis of all the four LEP experiments. It could not be explained via an SM-like Higgs boson because of a low production cross section. Considering the discovered Higgs boson to be  $H$  with  $m_H \sim 125$  GeV rather than  $h$ , MSSM in principle, in its non-decoupling domain can accommodate  $m_h$  at 98 GeV. Smaller  $\sin^2(\beta - \alpha)$ , consequently smaller  $hZZ$  or  $hWW$  couplings would be consistent with the LEP data whereas  $H$  with its SM-like couplings to vector bosons would provide us with consistent  $H \rightarrow \gamma\gamma$  and  $H \rightarrow ZZ^* \rightarrow 4l$ , the four-lepton decay channels. In a pre-LHC period, such a possibility of having  $m_h \sim 98$  GeV in the context of the LEP data was analyzed in Ref. [20]. In the recent time, in the “*post-Higgs at 125 GeV*” scenario the above Inclusive LEP-LHC Higgs perspective of assuming  $m_h$  at 98 GeV along with  $m_H$  at 125 GeV in the context of MSSM was analyzed in Refs. [21–23]. We will refer the above as “**Inclusive LEP-LHC Higgs**” (**ILLH**) scenario in this analysis. After the Higgs discovery announcement in the summer of 2012, there have been a few studies on NMSSM [24] which could easily accommodate the above ILLH physics [25, 26]. There also have been a few analysis that reported results in multiple Higgs bosons near 125 GeV [27] or a combined LHC plus Tevatron scenario of a 125 GeV plus a 136 GeV Higgs bosons [28], both in the context of NMSSM.

After the analyses of the Refs. [21–23], stronger constraints came from CMS [29] and ATLAS [30] for the decay of neutral Higgs bosons ( $H/A$ ) to  $\tau$  pairs. In MSSM, CMS data excludes parameter

zones with  $90 < M_A < 250$  GeV for  $\tan\beta$  approximately above 5.5. As pointed out in Ref. [31] there is a drastic reduction in the above limit of  $\tan\beta$  for the same range of  $M_A$  in comparison to the older result of 2011 [32]. This forces us to concentrate our search of the ILLH scenario for  $\tan\beta \lesssim 5.5$ . On the other hand, we must take into account the ATLAS analyzed constraint coming from  $t\bar{t}$  events, where  $t \rightarrow bH^+$  with  $H^+ \rightarrow \tau^+\nu_\tau$  [33]. This analysis indicates that, approximately for  $\tan\beta$  between 2 to 6, parameter regions satisfying  $90 < m_{H^+} < 150$  GeV become disallowed. Thus focusing on the two constraints from  $A/H \rightarrow \tau^+\tau^-$  and  $H^+ \rightarrow \tau^+\nu_\tau$ , we look for the ILLH scenario for a small range of  $\tan\beta$  namely  $3 < \tan\beta < 5.5$ . The lower limit of  $\tan\beta = 3$  is chosen so as to be consistent with Ref. [33]<sup>2</sup>. With the range of  $\tan\beta$  to be searched becoming restricted as mentioned above in the aforesaid non-decoupling region of MSSM for the ILLH scenario, one would require i)  $\sin^2(\alpha - \beta)$  to be sufficiently small so as to have a small  $Zh$  coupling in order to account for the 98 GeV data from LEP and ii) the heavier CP-even Higgs bosons  $H$  to be SM-like and be consistent with the LHC signals in di-photon, 4-lepton and  $WW^*$  channels. We also consider various low energy constraints. One of the most important constraints is  $Br(B_s \rightarrow \mu^+\mu^-)$  [35, 36] simply because of its inverse quartic relationship with the pseudoscalar mass  $M_A$ . Besides, we explore the role of other relevant constraints like  $Br(b \rightarrow s\gamma)$  [37] and  $Br(B \rightarrow \tau\nu_\tau)$  [38, 39]. We will also impose the cold dark matter (CDM) [40] constraint from PLANCK experiment [41] and compute the direct detection cross section of the lightest supersymmetric particle (LSP) for scattering with a proton in relation to the results of the XENON100 experiment [42]. However, we ignore the constraint due to muon  $g - 2$  in this analysis because although the deviation from SM is large, there are uncertainties in the evaluations of the hadronic contributions leading to significantly varying final limits [43].

We plan our analysis to proceed in the following way. In Section-2 we discuss the MSSM parameter scan strategy along with discussing different constraints to be imposed. In Section-3 we show the results of our scanning in MSSM parameter space in the light of the ILLH scenario along with a discussion on the most significant constraints on the MSSM Higgs sector. In the same section, we then move on to discuss the possibility of having 98 GeV as well as 125 GeV Higgs bosons in NMSSM. In Section-4, we discuss the collider implications of this scenario and finally in Section-5 we summarize our results.

---

<sup>2</sup>This is consistent with the LEP data analysis of Ref. [34] which however corresponds to an SM-like SUSY Higgs boson. For a 98 GeV non-SM like Higgs boson  $h$ ,  $\tan\beta$  can indeed be smaller than 3. Thus a much general analysis may probe smaller values of  $\tan\beta$  than 3.

## 2 Probing MSSM parameter space for ILLH Scenario

As mentioned earlier, although the MSSM Higgs sector is specified only by a few parameters like  $M_A$  and  $\tan\beta$ , it is due to the large radiative corrections to the Higgs boson masses several MSSM parameters, particularly the ones associated with the stop sector become important. The radiative corrections to  $\Delta m_h^2$  is quantified as follows [9, 44, 45].

$$\Delta m_h^2 = \frac{3\bar{m}_t^4}{2\pi^2 v^2 \sin^2\beta} \left[ \log \frac{M_S^2}{\bar{m}_t^2} + \frac{X_t^2}{2M_S^2} \left( 1 - \frac{X_t^2}{6M_S^2} \right) \right]. \quad (1)$$

Here,  $M_S = \sqrt{\bar{m}_{\tilde{t}_1} \bar{m}_{\tilde{t}_2}}$ ,  $v = 246$  GeV,  $X_t = A_t - \mu \cot\beta$  and  $\bar{m}_t$  refers to the running top-quark mass.  $A_t$  stands for trilinear coupling for top-quark given at the electroweak scale. The running top-quark mass also includes QCD and electroweak corrections. One must however include the radiative corrections from sbottom and stau sectors for cases with large  $\tan\beta$  and/or very large  $\mu$ . The importance of the latter comes from a  $|\mu|^4$  dependence [46]. We will particularly scan MSSM parameter space reaching up to large values of  $|\mu|$  without being concerned with any fine-tuning issue. Hence, the contributions at least from the sbottom sector are hardly negligible. Expressions of radiative corrections for heavier neutral Higgs bosons and charged Higgs bosons may be seen in Ref. [9].

With the above importance of Higgs related parameters of MSSM connected to radiative corrections for Higgs masses and the fact that we also would like to explore the parameter space that satisfy the XENON100 data [42], we select the following parameter ranges for scanning of MSSM parameter space. We point out that many of the parameters that are important to satisfy the CDM relic density [40, 47] constraints do not have significant effects on the Higgs sector or strongly interacting sectors that are relevant for Higgs [48]. For simplicity, we consider the squark masses of the first two generations as well as slepton masses of all the three generations sufficiently heavy. This will obviously not affect the Higgs masses whereas it will only avoid the possibility of LSP-slepton coannihilation scenarios for CDM constraint without any loss of generality. We generate approximately 70 million random points in the following combined range of parameters.

$$\begin{aligned} 3 < \tan\beta < 5.5, \quad 0.085 < M_A < 0.2 \text{ TeV}, \quad 0.3 \text{ TeV} < \mu < 12 \text{ TeV}, \\ 0.05 \text{ TeV} < M_1, M_2 < 1.5 \text{ TeV}, \quad 0.9 \text{ TeV} < M_3 < 3 \text{ TeV}, \\ -8 \text{ TeV} < A_t < 8 \text{ TeV}, \quad -3 \text{ TeV} < A_b, \quad A_\tau < 3 \text{ TeV}, \quad A_u = A_d = A_e = 0, \\ 0.3 \text{ TeV} < M_{\tilde{q}_3} < 5 \text{ TeV}, \quad \text{where, } \tilde{q}_3 \equiv \tilde{t}_L, \tilde{t}_R, \tilde{b}_L, \tilde{b}_R \\ M_{\tilde{q}_i} = 3 \text{ TeV, for } i = 1, 2 \quad \text{and} \quad M_{\tilde{l}_i} = 3 \text{ TeV, for } i = 1, 2, 3. \end{aligned} \quad (2)$$

Among the SM parameters, we consider  $m_b^{\overline{\text{MS}}}(m_b) = 4.19$  GeV and  $m_t^{\text{pole}} = 173.3 \pm 2.8$  GeV.  $m_t^{\text{pole}}$  is varied within the above range following the argument of Ref. [49]. We scan the parameters within

the above ranges of Eq.2 while imposing lower limits on the sparticle masses [50] and eliminating the possibility of having any charge and color breaking (CCB) minima [51].

While sketching out the valid parameter space we also consider the errors in the masses of two CP-even neutral Higgs bosons. We consider a theoretical uncertainty amount of 3 GeV in the Higgs mass computation that arises out of uncertainties in the renormalization scheme, scale dependence, the same in higher order loop corrections up to three loops or that due to the top-quark mass [15, 52–55]. Thus, we isolate the parameter space with the following limits for the Higgs boson masses.

$$\begin{aligned} 95 \text{ GeV} < m_h < 101 \text{ GeV}, \text{ and} \\ 122 \text{ GeV} < m_H < 128 \text{ GeV}. \end{aligned} \quad (3)$$

We further require  $h$  to have non-SM like couplings by demanding  $\sin^2(\beta - \alpha)$  to be small. The observed LEP excess [19] approximately results into:

$$0.1 < \sin^2(\beta - \alpha) < 0.25. \quad (4)$$

We now focus on the primary production channels of Higgs boson at the LHC and define the following ratios related to the gluon-gluon fusion and the vector boson fusion channels.

$$R_{gg}^{h,H}(XX) = \frac{\Gamma(h, H \rightarrow gg)\text{Br}(h, H \rightarrow XX)}{\Gamma(h_{SM} \rightarrow gg)\text{Br}(h_{SM} \rightarrow XX)} \quad (5)$$

and

$$R_{Vh/H}^{h,H}(YY) = \frac{\Gamma(h, H \rightarrow WW)\text{Br}(h, H \rightarrow YY)}{\Gamma(h_{SM} \rightarrow WW)\text{Br}(h_{SM} \rightarrow YY)}. \quad (6)$$

where,  $XX = \gamma\gamma$  or  $ZZ^*/W^+W^-$  and  $YY = b\bar{b}$  or  $\tau^+\tau^-$ . As we know that the production of Higgs at the LHC is dominated by gluon-gluon fusion both in the context of SM, as well as in our parameter zone of interest of MSSM. However, detection of Higgs bosons via  $h, H \rightarrow b\bar{b}$  and  $h, H \rightarrow \tau^+\tau^-$  decays becomes nearly impossible when the Higgs boson is produced via gluon-gluon fusion since it is likely to be overshadowed by di-jet events from QCD interactions. On the other hand, when Higgs boson is produced in association with a vector boson ( $W/Z$ ), also known as Higgs-strahlung (HS), with the gauge bosons decaying leptonically, it is relatively easy to tag the two  $b$ -jets to reconstruct the Higgs mass. Both ATLAS and CMS have probed Higgs signatures in this channel but with large uncertainties, which one would expect to be modified with enough data collected at the 14 TeV LHC run. Hence, we consider the Higgs-strahlung process when computing  $R_{Vh/H}^{h,H}(b\bar{b})$  for Higgs boson signals decaying into pair of bottom quark. Because of large uncertainties in these channels we refrain ourselves from imposing any limit on  $R_{VH}^H(b\bar{b})$  or

$R_{VH}^H(\tau^+\tau^-)$  in our analysis. Rather, we only set a lower limit for  $R_{gg}^H(\gamma\gamma)$ :

$$R_{gg}^H(\gamma\gamma) > 0.5.^3 \quad (7)$$

We now consider various low energy constraints. The experimental data from  $Br(b \rightarrow s\gamma)$  almost saturates the SM value that comes from  $t-W$  loop [56]. Within MSSM, the dominant contributions come from  $t-H^\pm$  and  $\tilde{t}_{1,2}-\tilde{\chi}_{1,2}^\pm$  loops [57], the former having the same sign as that of the  $t-W$  loop of SM. The chargino loop contribution is proportional to  $A_t\mu \tan\beta$ . Depending on the sign of  $A_t\mu$ , there can be cancellation or enhancement between the above loop contributions within MSSM [58]. Furthermore, we note that in SUSY,  $Br(b \rightarrow s\gamma)$  may have an indirect but important contribution from a gluino-squark loop at the next-to-leading order level. This is primarily connected to the renormalization of Yukawa couplings to down type of fermions. The corrections that can be summed to all order in perturbation theory relates to the supersymmetric quantum chromodynamic (SQCD) corrections to the mass of the bottom quark  $m_b$  and this is proportional to  $\mu M_{\tilde{g}} \tan\beta$  [58, 59]. This leads to alteration of the  $\bar{t}bH^+$  vertex leading to a correction to  $Br(b \rightarrow s\gamma)$  that comes with an opposite sign with respect to the leading order contribution of the  $t-H^\pm$  loop [58]. Typically, the correction is seen as a required one for large values of  $\tan\beta$ . But in spite of  $\tan\beta$  being small in our analysis, the same correction is also very important because of large possible values for  $\mu$  [59]. This next-to-leading order effect can potentially cancel the leading order effects from chargino or charged Higgs loops<sup>4</sup>. The experimental result is  $Br(b \rightarrow s\gamma) = (343 \pm 22) \times 10^{-6}$  [37] which at  $3\sigma$  level leads to:

$$2.77 \times 10^{-4} < Br(b \rightarrow s\gamma) < 4.09 \times 10^{-4}. \quad (8)$$

Next, as mentioned before, we must explore the effect of the limits from  $B_s \rightarrow \mu^+\mu^-$  particularly because of its  $M_A^{-4}$  dependence while we probe a light  $M_A$  scenario. The experimental (LHCb) and SM values are given by  $Br(B_s \rightarrow \mu^+\mu^-)_{exp} = (3.2_{-1.2}^{+1.4}(\text{stat.}) \pm 0.5(\text{syst.})) \times 10^{-9}$  [35]. This is to be compared with the SM result  $Br(B_s \rightarrow \mu^+\mu^-)_{SM} = (3.23 \pm 0.27) \times 10^{-9}$  [60]. As in Ref. [61], we combine the errors of LHCb data and SM result to obtain the following  $2\sigma$  limits.

$$0.67 \times 10^{-9} < Br(B_s \rightarrow \mu^+\mu^-) < 6.22 \times 10^{-9}. \quad (9)$$

---

<sup>3</sup>The most significant change in the recent updates on LHC results at the Moriond-2013 conference is that CMS no longer observes the excess in the di-photon channel from their multivariate analysis. However, a small excess is still there in their cut-based analysis. Moreover, ATLAS observes some excess in the di-photon mode (see Table 1 for details). Therefore, we choose a conservative limit of  $R_{gg}^H(\gamma\gamma) > 0.5$  which is within  $1\sigma$  of the CMS di-photon result (multivariate analysis).

<sup>4</sup>SUSY electroweak corrections to bottom Yukawa couplings may also be somewhat appreciable for very large values of  $\mu M_2$  [59].



We also take into account the combined constraint from  $Br(B^+ \rightarrow \tau^+ \nu_\tau)$  from BABAR [39] and  $Br(B^- \rightarrow \tau^- \bar{\nu}_\tau)$  from Belle [62]. With  $R_{(B \rightarrow \tau \nu_\tau)} = \frac{Br(B \rightarrow \tau \nu_\tau)_{SUSY}}{Br(B \rightarrow \tau \nu_\tau)_{SM}}$ , we find  $0.31 < R_{(B \rightarrow \tau \nu_\tau)} < 2.10$  (see Ref. [63] for details). Typically, the above constraint may be effective for large  $\tan \beta$  and smaller charged Higgs boson mass. The limits of  $R_{(B \rightarrow \tau \nu_\tau)}$  however do not impose any significant constraint on the parameter space of our study.

Finally, we take into account the CDM relic density limits recently provided by the PLANCK [41] collaboration, which at  $3\sigma$  level reads,

$$0.112 < \Omega_{\tilde{\chi}_1^0} h^2 < 0.128. \quad (10)$$

We also compute spin-independent direct detection LSP-proton scattering cross-section and compare with the XENON100 data [42]. The spin-independent cross section depends on t-channel Higgs and s-channel squark exchanges of which the former dominates unless the squark masses are close to that of the LSP [64,65]. We note that in a thermal production scenario of dark matter we may have the following possibilities: i) either the lightest neutralino constitutes the entire CDM relic density while corresponding to correct relic abundance satisfying PLANCK data or ii) it is just one of the candidates of a multicomponent DM combination with obviously a smaller relic density contribution from its own, below the lower limit of Eq.10. For the latter scenario one has  $\Omega_{\tilde{\chi}_1^0} h^2 < (\Omega_{CDM} h^2)_{\min}$ , where  $(\Omega_{CDM} h^2)_{\min}$  refers to the lower limit of Eq.10. Here, we should multiply with the fraction  $\zeta = \rho_\chi / \rho_0$  the LSP contributes to the total local density of DM to obtain the true event rate where  $\rho_0$  denotes the local total DM density and  $\rho_\chi$  means the DM density contributed by the LSP. Thus, one conveniently defines the ratio as  $\zeta = \min\{1, \Omega_{\tilde{\chi}_1^0} h^2 / (\Omega_{CDM} h^2)_{\min}\}$  [66].  $\zeta$  by definition is unity for scenarios with right abundance (single component) or over-abundance of DM.

## 3 Results

### 3.1 MSSM

We search for the ILLH scenario within the phenomenological MSSM parameter space corresponding to Eq.2. We use the code SuSpect (version 2.41) [67] for generating sparticle spectra and micrOMEGAs (version 2.4.5) [68–70] to compute neutralino relic density, LSP-nucleon direct detection cross-section as well as various B-physics related quantities. We compute relevant Higgs decays by using the code SUSY-HIT [71].

In Fig.1 we show the result of our parameter space scanning in  $M_A - \tan \beta$  plane. The results show parameter points in the above plane that satisfy i) the sparticle mass lower limits including those from LHC, ii) the two neutral CP-even Higgs boson masses  $m_h$  and  $m_H$  to be within the



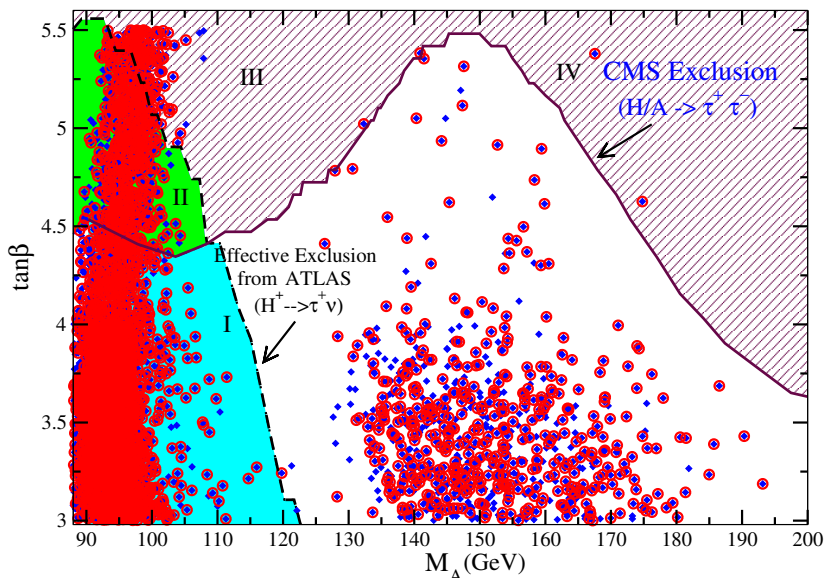


Figure 1: Scatter plot of mass of pseudoscalar Higgs boson  $M_A$  vs  $\tan\beta$  in the ILLH scenario of MSSM. The diamond (blue) shaped points satisfy the constraints of Eqs.3 to 9. The (red) circles (enclosing diamonds) additionally satisfy the DM relic density constraint. The shaded region above the solid (maroon) line is discarded via CMS data of  $H/A \rightarrow \tau^+\tau^-$ . The region below the dashed line is discarded via the indirect effect of the  $H^+ \rightarrow \tau^+\nu_\tau$  constraint from ATLAS. This is done by translating the constraint into the  $M_A - \tan\beta$  plane by using the tree level relationship between the masses of pseudoscalar and charged Higgs bosons in MSSM.

ranges of Eq.3, iii) the LEP specified limits for  $h$ -boson to be non-Standard Model like as in Eq.4 and iv) the chosen value  $R_{gg}^H(\gamma\gamma) > 0.5$ . Besides the above, the parameter points also satisfy limits for  $Br(b \rightarrow s\gamma)$  as shown in Eq.8 and the LHCb limits of  $Br(B_s \rightarrow \mu^+\mu^-)$  of Eq.9. We have also verified the validity of the range of  $R_{(B \rightarrow \tau\nu\tau)}$  as mentioned in the last section. The scattered points that satisfy the above limits are shown with diamond label (in blue). The red circles (enclosing diamonds) additionally show the points that satisfy the DM relic density constraint. In this analysis we consider the possibility of LSP to be also a sub-dominant candidate of dark matter. Thus consistency with the CDM relic density constraint here means satisfying only the upper limit of Eq.10. There is a general absence of valid points in the region of  $110 \lesssim M_A \lesssim 125$  GeV. We will come back to this point in the discussion of Fig.2.

The recent results of decay of heavy neutral Higgs bosons  $H/A$  to  $\tau$  pairs from CMS [29] and ATLAS [30] keep only the small  $\tan\beta$  zone to be allowed for small  $M_A$  region ( $< 200$  GeV).

Because of the above data there is no allowed zone for  $\tan\beta > 5.5$  for  $M_A < 200$  GeV as shown by the black solid line of Fig.1. The dashed line, on the other hand, shows the indirect effect of  $H^+ \rightarrow \tau^+\nu_\tau$  [33] constraint from ATLAS when translated into the  $M_A - \tan\beta$  plane by using the tree level relationship between the masses of pseudoscalar and charged Higgs bosons in MSSM, namely  $M_{H^\pm}^2 = M_A^2 + M_W^2$ . The latter constraint eliminates  $M_A$  below 120 GeV. The regions marked by I,II,III and IV are thus discarded via  $H/A \rightarrow \tau^+\tau^-$  and  $H^+ \rightarrow \tau^+\nu_\tau$  data. Hence, the surviving  $M_A$  range for  $3 < \tan\beta < 5.5$ , as shown in Fig.1 is given by,

$$130 < M_A < 200 \text{ GeV}. \quad (11)$$

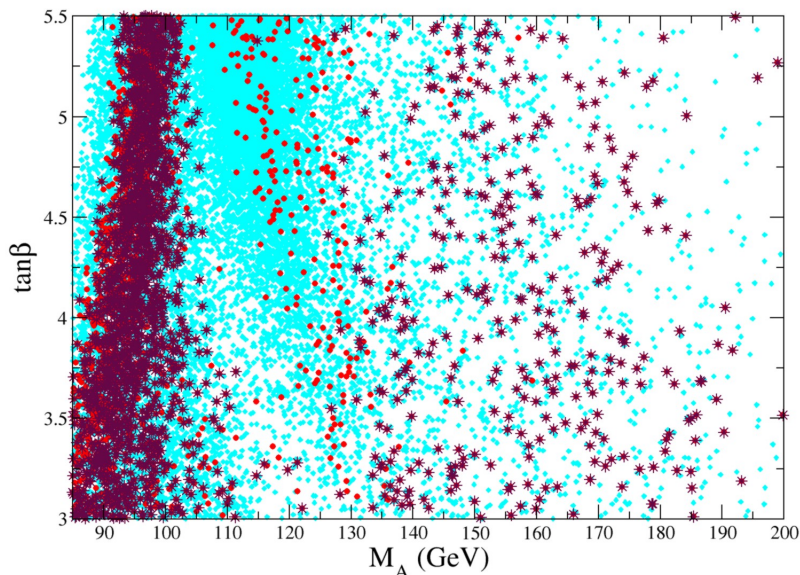


Figure 2: Scatter plot of mass of pseudoscalar Higgs boson  $M_A$  vs  $\tan\beta$  in the ILLH scenario of MSSM. The lightest (cyan) scattered points correspond to parameter points that at least satisfy the two Higgs mass constraints of Eq.3. Dark (red) filled circles correspond to imposing  $\sin^2(\beta - \alpha)$  limits from Eq.4. The star (maroon) shaped points are obtained by imposing  $Br(B_s \rightarrow \mu^+\mu^-)$  limits from Eq.9.

We now discuss the details of the interplay of the most important constraints of our analysis in the ILLH scenario of MSSM in the  $M_A - \tan\beta$  plane in regard to the blank intermediate zone  $110 \lesssim M_A \lesssim 125$  GeV as mentioned above. The lightest (cyan) scattered points of Fig.2 correspond to parameter points that at least satisfy the two Higgs mass constraints of Eq.3. The points in general span the  $M_A - \tan\beta$  plane, albeit with varying degree of existence for different zones. Imposing the LEP Higgs information regarding  $\sin^2(\beta - \alpha)$  from Eq.4 (shown as darker (red) circles) drastically reduces the available parameter space in the aforesaid intermediate zone of  $M_A$ . Further reduction

of parameter points in the same region occurs via the constraint of  $Br(B_s \rightarrow \mu^+ \mu^-)$  from Eq.9. The star (maroon) shaped points refer to parameter points in  $M_A - \tan \beta$  plane that satisfy Eq.9 in addition to Eqs.3 and 4. Thus the above step-by-step imposition of various constraints shows that requirement of  $h$ -boson to be non-SM like via Eq.4 and the stringent limits from  $Br(B_s \rightarrow \mu^+ \mu^-)$  (Eq.9) in combination cause the absence of valid points in the intermediate  $M_A$  zone (Fig.1).

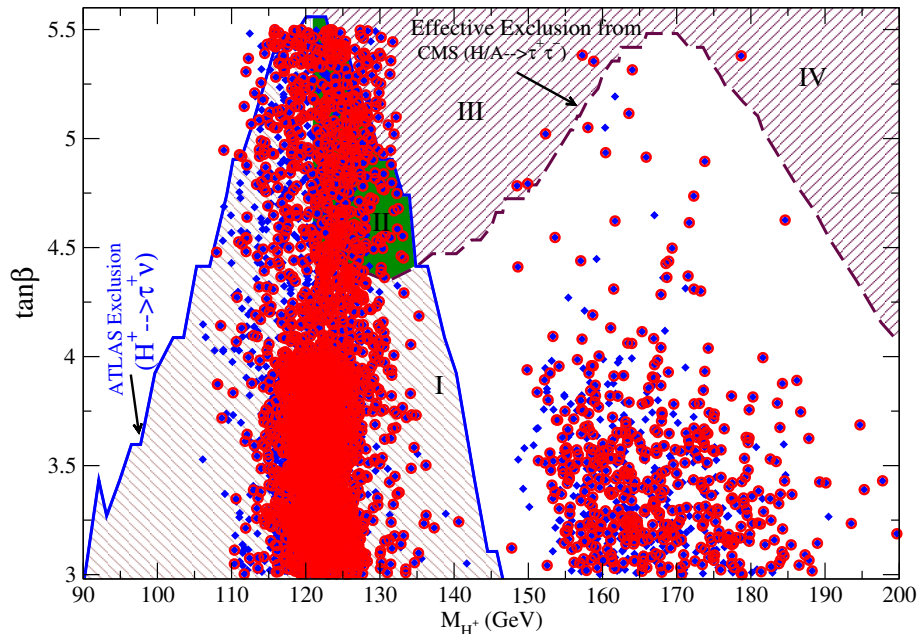


Figure 3: Scatter plot of mass of Charged Higgs boson  $M_{H^\pm}$  vs  $\tan \beta$  in the ILLH scenario of MSSM. Symbols have the same meaning as in Fig.1. Direct constraint from  $H^+ \rightarrow \tau^+ \nu_\tau$  from ATLAS is shown as a blue solid line. Indirect effect of  $H/A \rightarrow \tau^+ \tau^-$  from CMS is additionally drawn as a dashed (maroon) line by using the tree level relationship between  $M_A$  and  $M_{H^\pm}$ . All the shaded regions are discarded via the above two constraints.

Fig.3 shows a scatter plot in  $M_{H^\pm} - \tan \beta$  plane from same analysis. With similarly marked scattered points for the constraints as described above in connection with Fig.1, we draw direct constraint from  $H^+ \rightarrow \tau^+ \nu_\tau$  from ATLAS [33] as a blue solid line. The indirect effect of  $H/A \rightarrow \tau^+ \tau^-$  as seen in Fig.1 is additionally drawn as a dashed (maroon) line by using the tree level relationship between  $M_A$  and  $M_{H^\pm}$ . The region of  $M_{H^\pm} < 145$  GeV becomes entirely disallowed via  $H^+ \rightarrow \tau^+ \nu_\tau$  from ATLAS. The combined disallowed zones are shown as regions I to IV. The valid zone of charged Higgs mass is seen to be  $150 \text{ GeV} < M_{H^\pm} < 200 \text{ GeV}$  that falls below the line corresponding to

$H/A \rightarrow \tau^+\tau^-$  data from CMS [29].

### 3.1.1 Interplay of parameters related to Higgs mass radiative corrections: identifying most significant constraints

We now consider studying the parameters connected to the Higgs mass radiative correction, that becomes highly relevant for the ILLH scenario. As discussed before, important corrections come from the top-stop as well as bottom-sbottom loops. The latter loops become important because of large range of values of  $\mu$  considered in this analysis (Eq.2). We will also see that effect of considering large  $\mu$  has an important consequence on the constraints of  $Br(b \rightarrow s\gamma)$ .

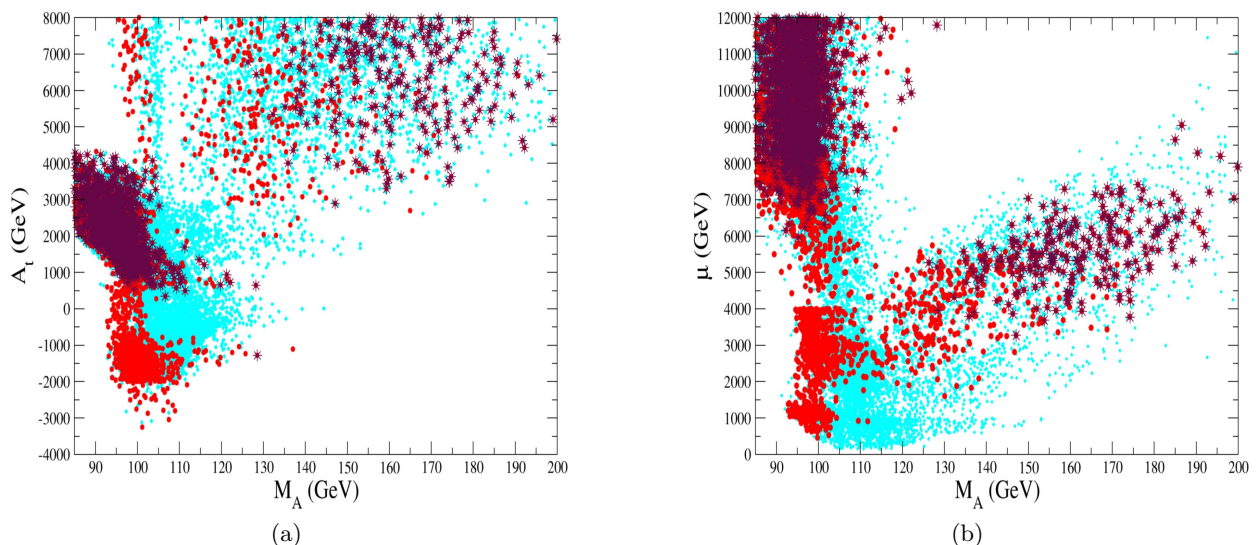


Figure 4: a) Scatter plot of mass of pseudoscalar Higgs boson  $M_A$  vs  $A_t$  in the ILLH scenario of MSSM. All the lightest (cyan) points satisfy at least the Higgs mass limits of Eq.3 and allow  $A_t$  to have either signs. Darker (red) circles additionally satisfy  $\sin^2(\beta - \alpha)$  limits from Eq.4. Star (maroon) marked points refer to further imposition of limits from  $Br(b \rightarrow s\gamma)$  and  $Br(B_s \rightarrow \mu^+\mu^-)$  corresponding to Eqs.8 and 9 respectively. This effectively discards negative values of  $A_t$ . b) Scatter plot of  $M_A$  vs  $\mu$  similarly obtained as Fig.4(a) with having same meaning for the symbols.

Fig.4(a) shows scattered points in the  $M_A - A_t$  plane. All the lightest (cyan) points satisfy at least the Higgs mass limits of Eq.3. These points include both positive as well as negative values of  $A_t$ . We see that there are parameter points satisfying just the two Higgs mass limits for negative values of  $A_t$  when  $M_A$  spans approximately up to 130 GeV. On the other hand, only positive solutions of  $A_t$  are available that satisfy the two constraints for  $M_h$  and  $M_H$  for larger values of  $M_A$  that are consistent with Eq.11. Further imposition of the LEP Higgs information regarding  $\sin^2(\beta - \alpha)$

from Eq.4 results into darker (red) circles which are also understood to coexist with star (maroon) marked points that additionally obey the constraints of  $Br(b \rightarrow s\gamma)$  and  $Br(B_s \rightarrow \mu^+\mu^-)$  (Eqs.8 and 9). Fig.4(b) shows the effect in  $M_A - \mu$  plane while constraints are imposed step-by-step as in Fig.4(a) with the symbols having the same meaning. Clearly, satisfying the two Higgs limits is possible both for small and large values of  $\mu$ . However like Fig.4(a) constraints from  $Br(b \rightarrow s\gamma)$  and  $Br(B_s \rightarrow \mu^+\mu^-)$  discard a large region of parameter space. For the surviving zone of Eq.11 the above selects a zone with relatively small values of  $\mu$  (up to 6 TeV ) (Fig.4(b)) as valid parameter range. Investigation reveals that it is indeed the limits from  $Br(b \rightarrow s\gamma)$  that disallow a large region of parameter space and we try to explain this in a brief *qualitative* detail by dividing the span of  $M_A$  into two distinct zones **(i) below** and **(ii) above** 130 GeV for both the subfigures of Fig.4. The above is same as dividing into smaller and relatively larger  $M_{H^\pm}$  zones. We remind that  $t - H^\pm$  loop contributes to  $Br(b \rightarrow s\gamma)$  with the same sign as that of  $t - W$  loop of SM [58].

• **Smaller  $M_A$  zone ( $\lesssim 130$  GeV) with  $A_t < 0$  where  $Br(b \rightarrow s\gamma)$  exceeds the allowed limit:**

Focusing on the smaller half side of  $M_A$  (i.e. below 130 GeV) of Fig.4(a), analysis revealed that  $Br(b \rightarrow s\gamma)$  typically becomes larger than the upper limit of Eq.8 when  $A_t < 0$  (but there are some cases where the value goes below the lower bound too in our multi-dimensional parameter space of MSSM, as we will see below). It turns out that the same smaller  $M_A$  region of Fig.4(b) (i.e. the lower half side) that is also associated with negative values of  $A_t$  and for which  $Br(b \rightarrow s\gamma)$  exceeds the allowed limit typically corresponds to smaller values of  $\mu$ . Thus combining the results of the two subfigures of Fig.4 we find that for most of the parameter zones corresponding to the lower half of  $M_A$  and negative  $A_t$ , the values of  $|\mu A_t|$  are relatively small since both the components namely  $\mu$  and  $|A_t|$  are individually on the smaller side. Thus in spite of having  $\mu A_t < 0$ , an apparently favorable situation for cancellation of diagrams in  $Br(b \rightarrow s\gamma)$  analysis, the chargino-stop loop contribution is not sufficient to overcome the large charged Higgs contribution which is typically larger in the smaller  $M_A$  zone than what it would be for the larger  $M_A$  zone as described above. Thus  $Br(b \rightarrow s\gamma)$  limit is violated in its upper bound.

• **Smaller  $M_A$  zone with  $A_t < 0$  where  $Br(b \rightarrow s\gamma)$  is below the lower limit:**

As mentioned before, in the low  $M_A$  zone, additionally there are small regions of parameter space with negative  $A_t$  where  $Br(b \rightarrow s\gamma)$  may become lesser than the lower limit of Eq.8 in the region of a sufficiently large  $\mu$ . Thus chargino contribution may significantly neutralize the charged Higgs contribution but as mentioned in Section-2 there may be an important gluino-squark loop contribution which comes with an opposite sign wrt the charged Higgs contribution. The latter contribution which goes in tandem with the negative contribution from the chargino loop (while



$A_t < 0$ ) causes  $Br(b \rightarrow s\gamma)$  to go below the lower limit of Eq.8.

- **Smaller  $M_A$  zone with  $A_t > 0$ :**

Here the chargino and the charged Higgs loop contributions add up but the gluino contribution which is important for large  $\mu$  and/or large  $M_{\tilde{g}}$  has an opposite sign. Even with varying stop, chargino and gluino masses, parameter points with very large and positive values of  $A_t$  typically have exceedingly large values of  $Br(b \rightarrow s\gamma)$  unless  $\mu$  becomes sufficiently large to cause a large degree of cancellation via the gluino loop. Such cancellations are indeed indicated in both the panels of Fig.4 for the low  $M_A$  zone when the cluster of star marked points span from  $0 < A_t < 4$  TeV whereas  $\mu$  varies from 6 to 12 TeV satisfying both the limits of  $Br(b \rightarrow s\gamma)$  of Eq.8.

- **Larger  $M_A$  zone ( $\gtrsim 130$  GeV) where  $A_t$  is essentially all positive:** Here the parameter points that satisfy the two Higgs mass limits are such that  $A_t$  is essentially always positive (except an insignificant number of parameter points). The charged Higgs mass goes higher, hence its contribution is relatively small. Although  $A_t$  is in the larger side,  $\mu$  is relatively in the moderate zone. Thus the combined chargino plus charged Higgs contribution which have the same signs is not exceedingly large and is balanced by the gluino contribution which comes with a negative sign. Thus in this zone of  $M_A$ ,  $Br(b \rightarrow s\gamma)$  constraint is likely to be satisfied a fact which is consistent with the figures. It is also quite likely to have adjacent parameter points that would fall below or above the limits of  $Br(b \rightarrow s\gamma)$  of Eq.8 in this zone of  $M_A$ .

Finally, Fig.5(a) shows the possible values of the higgsino mixing parameter  $\mu$  in  $M_A - \mu$  plane when all the constraints (Eqs.3 to 10) are imposed. For the valid  $M_A$  zone of Eq.11 most of the scattered points correspond to values of  $\mu$  between 3.5 TeV to 6 TeV. Fig.5(b) shows the spread of the lighter top-squark mass in  $M_A - M_{\tilde{t}_1}$  plane. For the valid  $M_A$  zone satisfying Eq.11 we find the value of lighter top-squark mass to spread within  $400 \text{ GeV} < M_{\tilde{t}_1} < 1.6 \text{ TeV}$ , a significant part of the range may indeed be probed in the LHC.

### 3.1.2 Higgs decay channels

Now we compute few Higgs decay ratios of interest in our analysis. The latest results as announced in Moriond Conferences in La Thuile (March 2013) may be seen in Table 1 [72–77]. Fig.6 shows the result of the computation of  $R_{gg}^H(\gamma\gamma)$  and  $R_{Vh}^h(b\bar{b})$  for the given parameter space of the ILLH scenario of MSSM. Considering  $1\sigma$  limit of the CMS result of  $\tilde{h} \rightarrow \gamma\gamma$  from Table 1 we use a conservative lower bound for  $R_{gg}^H(\gamma\gamma)$ , namely  $R_{gg}^H(\gamma\gamma) > 0.5$ . The spread of  $R_{Vh}^h(b\bar{b})$  is consistent with the LEP excess [19] of Eq.4. The diamond (blue) shaped points refer to satisfying all the relevant constraints (as those from Eqs.3 to 9) except the DM constraint. The points denoted by red circles additionally satisfy the DM constraint. We note that the smallness of the value of

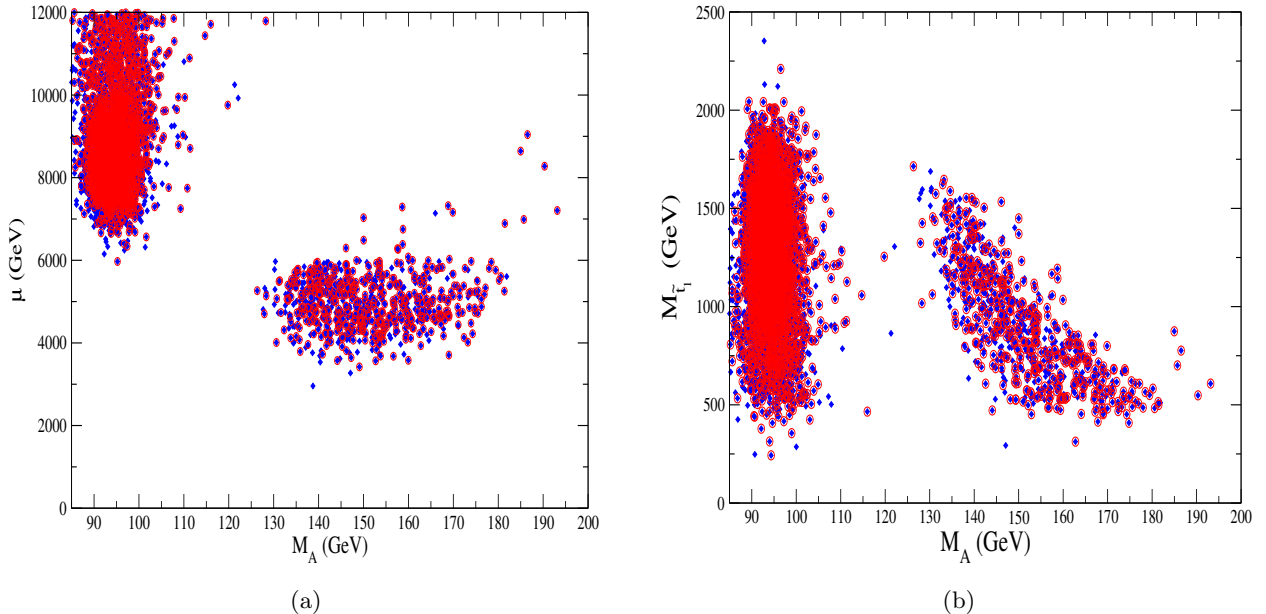


Figure 5: a) Scatter plot of mass of pseudoscalar Higgs boson  $M_A$  vs the Higgsino mixing parameter  $\mu$  in the ILLH scenario of MSSM and b) Scatter plot for  $M_A$  vs  $M_{\tilde{\tau}_1}$ . Symbols have same meaning as in Fig.1.

$R_{Vh}^h(bb)$  is consistent with the non-observability of  $h$  in Tevatron or in LHC [25] until now.

Fig.7(a) shows the scatter plot of  $R_{gg}^H(\gamma\gamma)$  vs  $R_{VH}^H(bb)$ , whereas Fig.7(b) shows the same for  $R_{gg}^H(\gamma\gamma)$  vs  $R_{VH}^H(\tau^+\tau^-)$  in the ILLH scenario of MSSM. Symbols have the same meaning as in Fig.6. We note that QCD and SUSY QCD corrections to  $m_b$  play important roles in modifying the total decay width as well as relevant branching ratios of  $H$ -boson [13, 17, 18].

### 3.1.3 Dark matter direct detection

We will briefly discuss now the cold dark matter relic density constraint. We only exclude the parameter points that lead to over-abundant relic densities, thereby we also include the cases where the LSP may be a sub-dominant component of dark matter. The parameter ranges of Eq.2 selected in our analysis are such that the principal mechanism to satisfy the relic density is  $\tilde{\chi}_1^0\text{-}\tilde{\chi}_1^\pm$  coannihilation where  $\tilde{\chi}_1^0$  is almost a pure bino and  $\tilde{\chi}_1^\pm$  is almost a pure wino. This happens for more than 99% of parameter points satisfying the upper limit of Eq.10. Very few parameter points (less than 1%) are associated with  $\tilde{\chi}_1^0\text{-}\tilde{t}_1$  coannihilation so as to reduce the relic density for a typically bino dominated LSP to an acceptable value. We note that our parameter ranges as mentioned in Eq.2 have heavy sleptons that naturally would not undergo any coannihilation with LSPs. We explore the detection prospect of the LSP in Fig.8(a) by computing the spin-independent direct



Higgs decay channel	Experiment	Signal strength
$h \rightarrow b\bar{b}$	Tevatron	$1.6 \pm 0.75$
$h \rightarrow \tau^+\tau^-$	CMS	$1.1 \pm 0.4$
$h \rightarrow \gamma\gamma$	ATLAS	$1.65^{+0.34}_{-0.30}$
$h \rightarrow \gamma\gamma$	CMS	$0.78^{+0.28}_{-0.26}$
$h \rightarrow WW^*$	ATLAS	$1.01 \pm 0.31$
$h \rightarrow ZZ^*$	ATLAS	$1.5 \pm 0.4$

Table 1: *Higgs decay channels, Experiments and Signal strengths.*

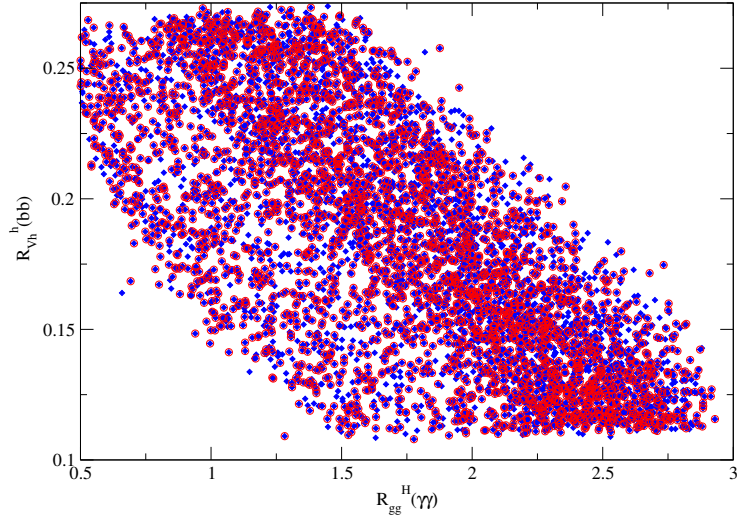


Figure 6: *Scattered plot of  $R_{gg}^H(\gamma\gamma)$  vs  $R_{Vh}^h(bb)$  in the ILLH scenario of MSSM. The diamond (blue) shaped points satisfy the constraints of Eqs.3 to 9. The (red) circles (enclosing diamonds) additionally satisfy the DM relic density constraint.*

detection  $\tilde{\chi}_1^0 - p$  cross-section using micrOMEGAs (version 2.4.5) [68–70] with default input values for direct detection. A considerable region above the solid (black) line is discarded via XENON100 data [42]. Here the diamond (blue) marked points refer to parameter points that satisfy all the relevant constraints of Eqs.3 to 9 except that they may or may not satisfy the DM relic density constraint. Circles (red) refer to satisfying only the upper limit of DM relic density of Eq.10 in addition to satisfying the constraints same as those of the diamond (blue) marked points. We extend our analysis in Fig.8(b) by computing the scaled cross-section  $(\zeta\sigma_{p\tilde{\chi}_1^0}^{SI})$  since most of the parameter

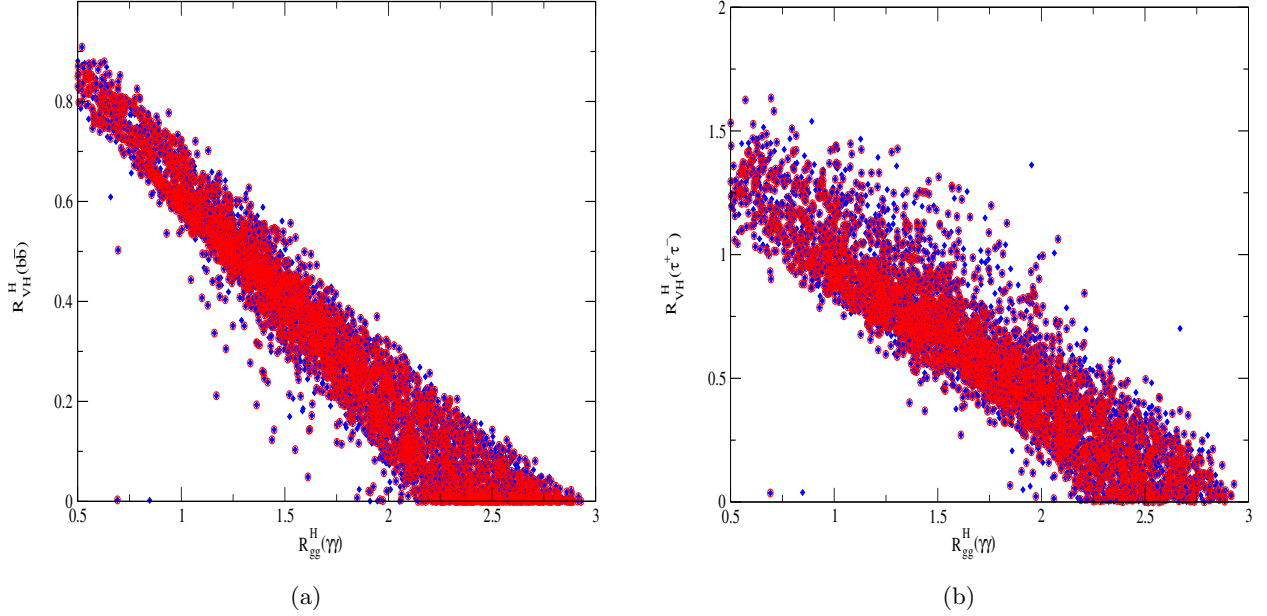


Figure 7: a) Scatter plot of  $R_{gg}^H(\gamma\gamma)$  vs  $R_{VH}^H(b\bar{b})$  in the ILLH scenario of MSSM. Symbols have the same meaning as in Fig.6. b) Scatter plot of  $R_{gg}^H(\gamma\gamma)$  vs  $R_{VH}^H(\tau^+\tau^-)$  in the ILLH scenario of MSSM. Symbols have the same meaning as in Fig.6.

points correspond to under-abundant relic densities. Here,  $\zeta = \min\{1, \Omega_{\tilde{\chi}_1^0} h^2 / (\Omega_{CDM} h^2)_{\min}\}$  [66], where  $(\Omega_{CDM} h^2)_{\min}$  refers to the lower limit of Eq.10. Clearly a significant amount of parameter space will be probed in future direct-detection experiment XENON-1T [78]. In Table 2 we show an example benchmark point for the ILLH scenario in MSSM in relation to Eq.2.

$M_t$	$M_A$	$\tan\beta$	$\mu$	$M_1$	$M_2$	$M_3$	$A_t$	$A_b$
173.6	167.5	5.0	5429.8	527.9	119.2	1416.6	5729.2	-217.1
$A_\tau$	$M_{\tilde{q}_{3L}}$	$M_{\tilde{t}_R}$	$M_{\tilde{b}_R}$	$M_h$	$M_H$	$M(H^\pm)$	$M_{\tilde{t}_1}$	$M_{\tilde{b}_1}$
-115.2	1712.6	1602.2	426.7	97.7	125.1	182.1	999.2	539.1
$M_{\tilde{g}}$	$\text{BR}(B_s \rightarrow \mu^+ \mu^-)$	$\text{BR}(b \rightarrow s\gamma)$	$\Omega h^2$	$\zeta \sigma_{(p-\chi)}^{SI}$				
1608.9	$2.8 \times 10^{-9}$	$3.8 \times 10^{-4}$	$4.5 \times 10^{-4}$	$5.5 \times 10^{-11}$				

Table 2: An example benchmark point for the ILLH scenario in MSSM in relation to Eq.2. All masses are in units of GeV.

In the next subsection we would like to extend our studies of the ILLH scenario to Next to Minimal Supersymmetry Model (NMSSM). However, before we move on to NMSSM Higgs sector, we would like to highlight the main issues of our analysis in MSSM:

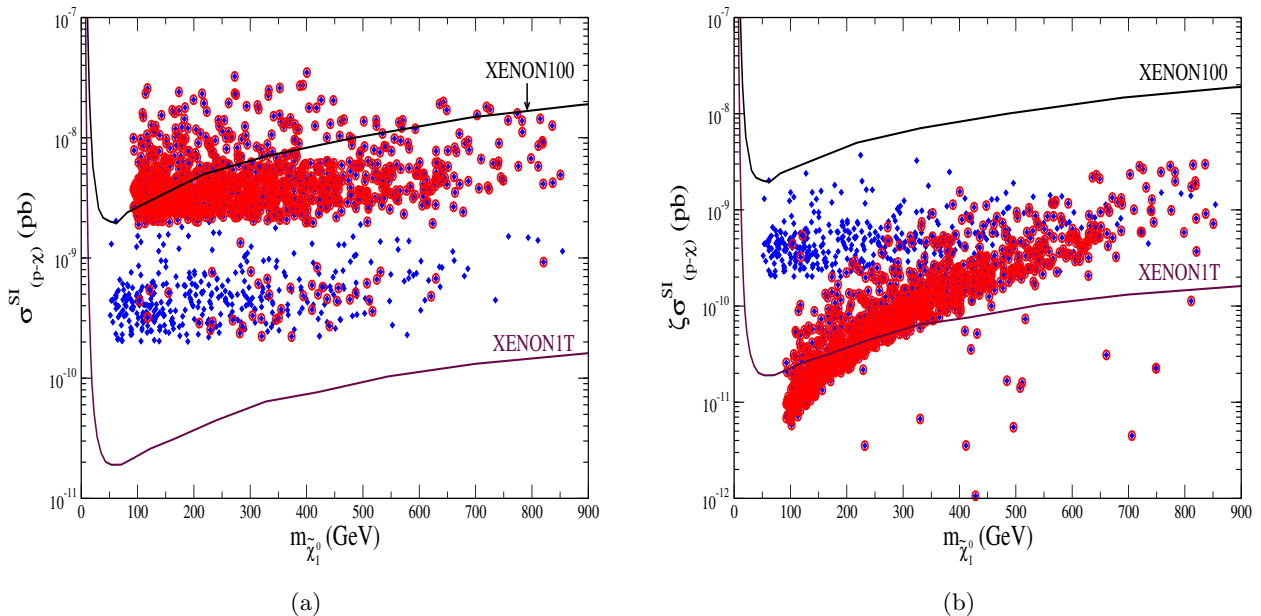


Figure 8: a) Scatter plot of  $m_{\tilde{\chi}_1^0}$  vs the spin-independent proton- $\tilde{\chi}_1^0$  direct detection scattering cross-section  $\sigma^{SI}$  in the ILLH scenario of MSSM. The XENON100 and future experiment of XENON-1T constraints are shown as solid lines. Further details are mentioned in the text. b) Same as (a) except that  $\sigma^{SI}$  is rescaled to  $\zeta\sigma^{SI}$ , where  $\zeta = \min\{1, \Omega_{\tilde{\chi}_1^0} h^2 / (\Omega_{CDM} h^2)_{\min}\}$ .

- We have found that the constraints from CMS and ATLAS for the ILLH scenario where one can possibly have both 98 GeV as well as 125 GeV for the two Higgs boson masses restrict  $\tan\beta$ ,  $M_A$  and  $M_{H^\pm}$  to be within the following ranges:  $3 < \tan\beta < 5.5$ ,  $130 \text{ GeV} < M_A < 200 \text{ GeV}$  and  $150 \text{ GeV} < M_{H^+} < 200 \text{ GeV}$ .
- Parameters related to radiative corrections to the Higgs sector do have significant impact in our analysis. Additionally, constraint from  $Br(b \rightarrow s\gamma)$  plays an effective role to discard a large region of parameter space. Particularly this limits  $A_t$  to have only the positive branch and constrains  $\mu$  to assume values between 3.5 – 6 TeV for all the allowed points within the valid  $M_A$  zone satisfying Eq.11.

### 3.2 NMSSM

One can very easily extend MSSM to NMSSM by simply adding a gauge singlet superfield  $\hat{S}$  that couples with the Higgs doublets via an interaction  $\lambda\hat{S}\hat{H}_u\hat{H}_d$  in the superpotential apart from a self interaction term for  $\hat{S}$  namely,  $\frac{\kappa}{3}\hat{S}^3$  [24].  $\lambda$  is chosen so that the above interaction terms remains

perturbative up to the unification scale ( $M_G \sim 2 \times 10^{16}$  GeV) depending on  $\kappa$  and  $\tan\beta$ . For SUSY breaking, in addition to the MSSM soft-SUSY breaking terms, one considers scalar mass term corresponding to the singlet superfield  $\hat{S}$ , trilinear coupling terms  $\lambda A_\lambda H_u H_d S$  and  $\frac{1}{3}\kappa A_\kappa S^3$  along with their hermitian conjugates.

In NMSSM one expands around the vacuum with non-vanishing vevs of the neutral CP-even components of  $H_u$ ,  $H_d$  and  $S$ . The scalar component of superfield  $\hat{S}$  can mix with the neutral scalar components of  $\hat{H}_u$  and  $\hat{H}_d$ . This leads to three CP-even Higgs bosons  $H_i$ ,  $i = 1, 2, 3$  and two CP-odd neutral Higgs bosons  $A_i$ ,  $i = 1, 2$ . Similarly, the fermionic superpartner of  $\hat{S}$  mixes with the neutral fermionic superpartners of  $\hat{H}_u$  and  $\hat{H}_d$  along with the neutral electroweak gauginos leading to five neutralinos.

We consider a semi-constrained version of NMSSM [24] which is characterized by the following parameters to be given at  $M_{\text{GUT}}$ :

- Universal gaugino mass parameter  $M_{1/2}$ ,
- Common scalar (sfermion) mass parameter  $m_0$  except for the Higgs scalars. The Higgs soft mass terms  $m_{H_u}^2$ ,  $m_{H_d}^2$  and  $m_S^2$  are taken as non-universal, and
- Common trilinear coupling for top, bottom and tau:  $A_t = A_b = A_\tau \equiv A_0$ . The trilinear couplings  $A_\lambda$ ,  $A_\kappa$  may differ from  $A_0$ .

Thus, the complete parameter space is defined by

$$\lambda, \kappa, \tan\beta, \mu_{\text{eff}}, A_\lambda, A_\kappa, A_0, M_{\frac{1}{2}}, \text{ and } m_0. \quad (12)$$

Here,  $\mu_{\text{eff}} = \lambda \langle S \rangle$  where  $\langle S \rangle$  denotes the vev of the scalar part of the singlet superfield. We scan these parameters in the following ranges:

$$\begin{aligned} 0.1 < \lambda < 0.7, & & 0.05 < \kappa < 0.5, \\ 1 < \tan\beta < 10, & & 0.1 \text{ TeV} < \mu_{\text{eff}} < 0.5 \text{ TeV}, \\ 0.1 \text{ TeV} < m_0 < 3 \text{ TeV}, & & 0.1 \text{ TeV} < M_{\frac{1}{2}} < 3 \text{ TeV}, \\ -1 \text{ TeV} < A_\lambda < 1 \text{ TeV}, & & -1 \text{ TeV} < A_\kappa < 1 \text{ TeV}, \\ -6 \text{ TeV} < A_0 < 6 \text{ TeV}. & & \end{aligned} \quad (13)$$

The ranges of  $\lambda$ ,  $\kappa$ ,  $\mu_{\text{eff}}$ ,  $A_\lambda$  and  $A_\kappa$  are chosen so that the CP-even and the CP-odd Higgs boson masses may assume a wide range of values. The random scan of the above NMSSM parameter space to calculate the Higgs and the SUSY particle spectrum along with various couplings, decay widths and branching ratios, is performed by using the code NMSSMTools 3.2.4 [79, 80]. The dark matter

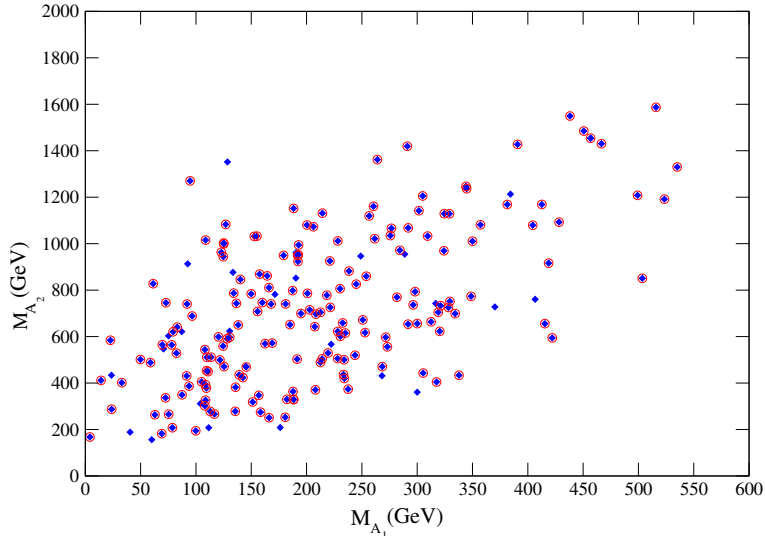


Figure 9: Scatter plot in  $M_{A_1} - M_{A_2}$  plane. Constraints imposed are same as MSSM and symbols have the same meaning as in Fig.1.

relic density and direct detection cross-section of the lightest neutralino  $\chi_1^0$  have been computed by using micrOMEGAs (version 2.4.5) [68–70] as implemented in the NMSSMTools. Similar to the analysis with MSSM, we impose the Higgs mass limits for  $m_{H_1}$  and  $m_{H_2}$  from Eq.3 where  $H_1$  here refers to the lighter CP-even Higgs boson. We also use all other constraints similar to what is done for MSSM.

Fig 9, shows the correlation between the pseudoscalar Higgs masses in  $M_{A_1} - M_{A_2}$  plane. Note that, in this parameter space of interest all other Higgs masses are almost degenerate i.e.  $M_{A_2} \sim M_{H_3} \sim M_{H^\pm}$ . Thus the above along with Fig.9 indicates that the masses of  $A_1$ ,  $A_2$  and  $H^\pm$  bosons may become much heavier than the corresponding Higgs bosons of MSSM. In fact, the charged Higgs boson may even be in the TeV range while  $A_1$  can be light and this is also true for heavy  $A_1$  [25]. This is a clear distinction in contrast to MSSM where it is very difficult to accommodate a 98 GeV Higgs boson with  $M_A$  larger than 200 GeV satisfying all the present collider bounds coming from the LHC data. (see Fig.1). In Section-3.1, we have shown that the 98 GeV Higgs boson scenario has been constrained to a very narrow region in the MSSM parameter space via  $A \rightarrow \tau^+\tau^-$  searches [29] in CMS and  $H^\pm \rightarrow \tau\nu_\tau$  searches in ATLAS [33]. However, the situation is different in the case of NMSSM. Here the above CMS data cannot be directly applied to constrain the parameter space associated with the ILLH scenario of Higgs Bosons. In NMSSM the experimental bounds on the decay of neutral Higgs bosons to a pair of  $\tau$ -lepton would not be effective enough to constrain the model because of the presence of doublet-singlet mixing in the NMSSM Higgs sector. In the following section we will discuss the discovery potential of light Higgs boson at the LHC.

## 4 Collider Prospects

In the previous two sections, we studied the possibility to accommodate a combination of a 98 GeV and a 125 GeV Higgs bosons in the non-decoupling limit of MSSM and in NMSSM. One attractive feature of the non-decoupling scenario of MSSM is that here all the Higgs bosons are relatively light and thus can be probed at the early run of the LHC. Hence, non-observation of these light Higgs bosons will of course indirectly exclude the possibility of a scenario with a 98 GeV Higgs boson. A dedicated analysis to explore this possibility at the 8 TeV and 14 TeV LHC run has been performed in Ref. [23] where  $M_A$  is varied between  $\sim 95$  to 130 GeV. It is to be noted that the above analysis relies on the presence of  $\tau$  from the decay of  $A$  or  $H^\pm$  bosons. However as seen in Fig.3 that for some region of the parameter space,  $H^\pm$  can be heavier than top quark and thus charged Higgs branching to  $H^\pm \rightarrow \tau^\pm \nu_\tau$  can be negligibly small. In other words, the above analysis is not applicable for  $M_H^\pm > M_t$  region and further study is required to exclude this region. As we found in Section-3.1 for MSSM results (Fig.1) the above range of  $M_A$  considered in Ref. [23] is now disfavored via the charged Higgs search by the ATLAS Collaboration [33]. The ATLAS search restricts the allowed points in the MSSM Higgs sector to be confined in the range  $130 \text{ GeV} < M_A < 200 \text{ GeV}$  for  $\tan\beta \sim 3 - 5.5$ .

NMSSM differs from MSSM because of an additional mixing in the Higgs sector arising from the singlet scalar in the model. Here, the lightest neutral CP odd Higgs boson can be light or heavy depending upon the choice of parameters (Fig.9). Besides, heavy scalars or mostly singlet scalars are also difficult to produce at the LHC. This implies that it is very hard to rule out a 98 GeV Higgs boson from indirect evidences, like non observation of other Higgs scalars. Hence, the exclusion/discovery of a 98 GeV Higgs boson is completely a model dependent phenomena and we need some way out to exclude this possibility in a model independent manner. We would like to stress the fact that a statistically significant  $2.3\sigma$  excess of events in the LEP experiments constrains the effective coupling  $g_{ZZH}^{BSM}$  leading to  $g_{ZZH}^{BSM}/g_{ZZH}^{SM} \simeq 0.3 - 0.5$ . We will see that the above range of the ratio in turn controls the Higgs production cross-section at LHC.

As mentioned previously, the primary Higgs boson production channels relevant at the LHC environment are gluon-gluon fusion. For  $m_H \leq 130\text{-}140$  GeV, the Higgs boson primarily decays to b-quarks, tau leptons, and  $WW^*/ZZ^*$ . It is particularly difficult to detect a 98 GeV Higgs boson produced via gluon-gluon fusion and decaying into bottom quarks because of large QCD jet background. Besides, if the Higgs decays to a pair of photons, it is again very hard to distinguish it from the continuous background due to its heavily suppressed branching ratio to a pair of photons ( $R_{gg}^H(\gamma\gamma) \sim 2 - 5\%$ ). One may also produce such a light Higgs boson via vector boson fusion process which then decays into a pair of  $\tau$ -lepton. The signal consists of two tagged forward jets and a pair

of  $\tau$ -leptons in the central rapidity region. It was shown that the detection of the Higgs boson via this channel is most sensitive for the Higgs mass in the vicinity of 130 GeV [81, 82]. Consequently, a VBF production mode would not be sensitive enough to detect a 98 GeV Higgs boson because of a large background. Hence, we ignore this production mode in rest of our analysis. The next most important production mode is the Higgs-strahlung process  $VH$  where the  $H$  is produced in association with a gauge boson  $W/Z$ . The Higgs-strahlung process  $VH$  in a boosted regime signifies that both the gauge bosons would have large transverse momenta. However, this boosted regime corresponds to a very small fraction of the total cross-section (about 5% for  $p_T^H > 200$  GeV, for  $m_H = 120$  GeV) [83] for a 14 TeV LHC run. On the other hand, the kinematic acceptance for this process is relatively large, whereas the backgrounds are small. The most important feature of a boosted particle decaying into multiple hadronic jets is that the final states remain highly collimated because of large transverse momenta of the parent particle. The latter appear as a single fat jet. Hence, conventional jet finding algorithms would not be sufficient enough to reconstruct the signal events. This realization has led to a new technique, called *Jet Substructure* [83] that studies new physics signatures involving hadrons in final states. This technique is based on the following sequential algorithm:

- Final state  $b$ -jets (from  $H \rightarrow b\bar{b}$ ) are formed based iterative jet clustering algorithm. Here we consider the Cambridge Aachen algorithm [84].
- Investigate subjet kinematics step-by-step.
- Choose the best subjets to form the fat jet mass which essentially corresponds to the parent Higgs particle.

Phenomenological analysis employing state-of-the-art jet substructure technique for highly boosted regime show that the Higgs-strahlung process could be a very promising search channel for a 120 GeV SM Higgs boson [83]. The ATLAS collaboration investigated this claim using a further realistic simulation [85]. The ATLAS analysis performed in three sub-channels based upon the decay of the vector boson considered the following.

1. Missing transverse momentum  $\cancel{p}_T > 30$  GeV and  $p_T^{e/\mu} > 30$  GeV consistent with a  $W$ -boson with  $p_T > p_T^{\min}$ .
2. Di-lepton invariant mass cut :  $80 \text{ GeV} < m_{\ell\ell} < 100 \text{ GeV}$ , where,  $\ell = e, \mu$  and  $p_T > p_T^{\min}$ .
3. Missing transverse energy  $\cancel{E}_T > p_T^{\min}$ .



Here,  $p_T^{\min}$  refers to the minimum transverse momentum of the Higgs required to call it a *Fat jet*. As in the ATLAS physics note of Ref. [85] we assume  $p_T^{\min} = 200$  GeV. The selection criteria (1) is mostly related to the process WH when W decays to a lepton ( $e/\mu$ ) and a neutrino, while (2) refers to the process HZ when Z-boson decays into a pair of lepton ( $e/\mu$ ). Item (3) selects the process HZ when Z-boson decays invisibly to a pair of neutrinos. Contribution from HW process may come for the sub-channel (3) when the lepton from W is outside the acceptance domain. We note that, (2) is a very clean signal but has a low cross-section while (1) and (3) have relatively higher signal cross-sections but these are mostly overshadowed by continuous  $t\bar{t}$  background. Using the prescribed procedure of ATLAS simulation, we have reproduced expected number of events with  $30 \text{ fb}^{-1}$  data for all the three signal subprocesses as presented in the Table 1 of the above-mentioned ATLAS physics note [85]. We have used Pythia6 (version 6.4.24) [86] for the generation of signal events and the package FASTJET (version 2.4.3) [87] for reconstruction of jets and implementation of the jet substructure analysis for reconstruction of the boosted Higgs. We present our final results in Table 3, where the background event numbers are appropriately scaled by using corresponding numbers given in the above ATLAS note. In order to satisfy the existing LEP bounds for the 98 GeV Higgs boson, we further assume a 20% LEP excess around the mass window 92 - 108 GeV. The expected number of events for signal and the various backgrounds for  $300 \text{ fb}^{-1}$  of collected data is listed in Table 3. The resulting statistical significance is presented in the fourth column of Table 3 considering the aforesaid mass window, whereas the last column represents the combined significance we obtained by adding the same for each channel in quadrature. We find that one can marginally exclude the presence of 98 GeV Higgs boson using  $300 \text{ fb}^{-1}$  of data at the 14 TeV LHC assuming only statistical uncertainty. However, at these high luminosity the pile ups, multiple interactions play a crucial role. Consequently estimation of signal significance would be limited due to large systematic uncertainties in the background calculations. On the other hand, backgrounds and selection cuts used in our analysis are taken from the above-mentioned ATLAS note [85]. These are not optimized for the 98 GeV Higgs boson, thus requiring further realistic analysis. From the above discussion one can infer that the model independent exclusion of a 98 GeV Higgs boson may not be possible even at the high luminosity run of LHC. However, if we are fortunate enough, we can even discover this particle via other processes. Let us survey the discovery potential of another production mode: the associated production of the 98 GeV Higgs with top quarks when the Higgs decays to a pair of bottom quark ( $pp \rightarrow t\bar{t}H, H \rightarrow b\bar{b}$ ). The production cross-section in this channel for a  $\sim 100$  GeV Standard Model Higgs is  $\sim 1$  pb at the 14 TeV run of LHC [88]. In a boosted regime, the decay products of both the top quarks and the Higgs would be highly collimated and jet substructure algorithm can be a very useful tool to tag top quarks

Process	Signal (S)	Background (B)	Significance ( $\frac{S}{\sqrt{B}}$ )	Combined Significance
$\ell\nu b\bar{b}$	35.6	417	1.7	
$\ell^+\ell^-b\bar{b}$	11.8	160.5	0.9	2.5
$\cancel{E}_T b\bar{b}$	54.6	1136	1.6	

Table 3: *Expected number of events at 14 TeV LHC run with  $300 \text{ fb}^{-1}$  of integrated luminosity within a mass window 92 - 108 GeV, based on LO cross sections, for the individual signal and the combined background processes assuming 20% LEP excess in this region of interest. The combined significance is obtained by adding significances in quadrature.*

and Higgs. Instead of reconstructing the individual top decay products, in *top tagging* which is a technique to identify boosted hadronic top quarks, one uses a jet algorithm and performs a subjet analysis to reconstruct the top quark mass. We would like to remind our readers that production cross section of this channel is highly parameter space dependent. Performing a random scan of the MSSM parameter space, we obtain  $R_{pp}^h(b\bar{b})$  to be within 20 to 60% where  $h$  refers to the 98 GeV Higgs boson of MSSM. However, with a conservative standpoint we choose  $R_{pp}^h(b\bar{b}) = 0.2$ . We do not perform any detailed analysis in this mode. Here we refer the results of an analysis already performed in this direction for a  $\sim 115$  GeV Standard Model Higgs boson at 14 TeV LHC [89]. While translating the results of Ref. [89] for our choice of Higgs mass, we expect an enhancement of 60% and 20% in the Higgs production rate and the background estimation respectively. Both these enhancements simply come from the difference in the choice of Higgs boson mass considered in Ref. [89] and ours. Hence, in our analysis we scale the signal and background by 1.6 and 1.2 respectively for a 98 GeV Higgs boson decaying to a pair of bottom quarks. It turns out that for an integrated luminosity of  $300 \text{ fb}^{-1}$  and a 98 GeV Higgs boson, with two tagged b-jets the statistical significance of this channel is  $\sim 3.1\sigma$ . On the other hand, for a three b-tag sample the significance is  $\sim 2.6\sigma$ . Again, we remind that the systematic uncertainty has not been taken into account.

Apart from these direct production mechanisms, the 98 GeV Higgs boson may be produced from the cascade decay of SUSY particles. From our scan of MSSM and semi-constrained NMSSM it comes out that squarks/gluinos are sufficiently heavy leading to very small strong production cross section. However, in a more general framework squark/gluinos can be light, just above the LHC specified limits. In that case, the decay of gauginos can produce highly boosted Higgs bosons which may be probed using the jet substructure technique (for details see [90–93] and references therein). Besides, a 98 GeV Higgs production from the decay of heavy Higgses may play an important role at the LHC [94, 95].

The proposed  $e^+e^-$  international linear collider (ILC) is an ideal machine to study this ILLH

scenario due to its clean environment and relatively less background contamination. The possibility to verify this ILLH scenario in the context of NMSSM in the Linear colliders have already been discussed in Ref. [25]. Here, the authors studied all the possible production/decay modes of NMSSM Higgs bosons in the context of Linear collider, Photon collider as well as Muon collider. However, our goal is to probe this scenario in a model independent way. Here we consider ILC with  $\sqrt{s}=250$  GeV and integrated luminosity  $=100 \text{ fb}^{-1}$ . The golden channel for the Higgs production in the context of ILC is  $e^+e^- \rightarrow ZH$ , where,  $Z$  can decay both leptonically or hadronically. The final state would involve jets and/or leptons depending upon the decay of the  $Z$ -boson while we assume Higgs always decays into a pair of bottom quark. We use MadGraph5 [96] to estimate the cross-section for both the signal and the SM background for  $100\text{fb}^{-1}$  luminosity. The production cross-section of a 98 GeV Standard Model Higgs boson at the ILC with 250 GeV center of mass energy is about 350 fb. The most dominant background comes from the  $Z$ -pair production which is about 1.1 pb. In order to satisfy the LEP bounds, we assume a 20% LEP excess for the 98 GeV Higgs boson. We further assume 60%  $b$ -tagging efficiency while calculating the statistical significance  $(S/\sqrt{B})$ . We find that a 98 GeV Higgs boson can be easily discovered/excluded at the 250 GeV ILC with a  $100 \text{ fb}^{-1}$  luminosity which is easily achievable within the first few years of its run.

## 5 Conclusion

To summarize, we have studied the possibility that both the LEP excess in  $b\bar{b}$  final state with a 98 GeV Higgs boson and the LHC di-photon signal for a 125 GeV Higgs-like object can be simultaneously explained in the general MSSM framework. It turned out that the MSSM parameter space where such scenario is valid is also consistent with several low energy constraints obtained from the heavy flavour sector, the cold dark matter constraints obtained from the recent PLANCK collaboration, limits from XENON100 experiment on the dark matter direct detection cross-section. In our MSSM Higgs parameter space scan we have also implemented the recent results on the heavy MSSM Higgs boson search via  $H/A \rightarrow \tau^+\tau^-$  mode from CMS and ATLAS collaboration and the search of charged Higgs boson from ATLAS via  $H^\pm \rightarrow \tau^\pm\nu_\tau$  mode. After all these constraints, we have finally obtained the following allowed ranges of  $M_A$  and  $M_{H^\pm}$ :  $130 \text{ GeV} < M_A < 200 \text{ GeV}$  and  $150 \text{ GeV} < M_{H^\pm} < 200 \text{ GeV}$ . We have also shown that for the above ranges of  $M_A$  and  $M_{H^\pm}$ ,  $\tan\beta$  is confined in a very narrow window  $\sim 3 - 5.5$  from the Higgs searches at the LEP and the LHC.

We have also pointed out that parameters related to radiative corrections to the Higgs spectrum have significant impact on our whole analysis. Additionally,  $Br(b \rightarrow s\gamma)$  limits discard a large region of parameter space and this we tried to explain in a reasonable detail. Particularly, this causes  $\mu$

to vary between 3.5 – 6 TeV for all the allowed points.

We have also studied the correlation between different decay modes ( $H \rightarrow \gamma\gamma, b\bar{b}, \tau\bar{\tau}$ ) of the heavy Higgs boson of MSSM ( $M_H \sim 125$  GeV) and our results showed that these rates are consistent within  $1\sigma$  of the latest data on the Higgs signal from 7 TeV and 8 TeV LHC run. Moreover, we have also discussed briefly the prospect of the ILLH scenario in the context of NMSSM. Indirect exclusion of a 98 GeV Higgs boson in NMSSM is possible though it depends on the choice of the model parameters and the particle spectrum.

We studied the possibility of observing the 98 GeV Higgs boson at the 14 TeV run of LHC. We focused on the 98 GeV Higgs production via Higgs-strahlung:  $pp \rightarrow VH$ , followed by  $H \rightarrow b\bar{b}$  decay. Because of the large  $p_T$  of such Higgs boson at the 14 TeV LHC, the decay products of the Higgs boson will form a highly collimated jet and we performed our analysis using the technique of jet substructure. Our analysis showed that the statistical significance for observing the above Higgs boson signal at the 14 TeV LHC run with  $300 \text{ fb}^{-1}$  luminosity is at most  $2.5\sigma$ . Moreover, when the Higgs boson is produced in association with top quarks one can achieve a  $3.1\sigma$  ( $2.6\sigma$ ) level of statistical significance with two (three) tagged  $b$ -jets. Here, we would like to stress that throughout the analysis we have not taken into account the systematic uncertainties in the SM background estimation which certainly would modify the signal significance. We hope that the experimental collaborations would perform more dedicated analysis in this direction using the real data of the 14 TeV run of LHC. We have also attempted to explore the prospect of ILC to probe ILLH Higgs scenario. Even with a very conservative estimate, ILC would have a much better sensitivity to exclude or discover the 98 GeV Higgs boson within a few years of its run.

## 6 Acknowledgments

B.B. and D.D. thanks Indian Association for the Cultivation of Science (IACS), India for hospitality when the initial part of work was done. B.B acknowledges the support of the World Premier International Research Center Initiative (WPI Initiative), MEXT, Japan. D.D. thanks Harish-Chandra Research Institute (HRI), Allahabad, India for hospitality in addition to the support received from the DFG, project no. PO-1337/3-1 at the Universität Würzburg. M.C. would like to thank the Council of Scientific and Industrial Research, Government of India for support. DKG would like to thank the Helsinki Institute of Physics, University of Helsinki, Finland for the hospitality during the final stage of this work.

## References

- [1] S. Chatrchyan *et al.* [CMS Collaboration], Phys. Lett. B **716**, 30 (2012) [arXiv:1207.7235 [hep-ex]]; S. Chatrchyan *et al.* [CMS Collaboration], arXiv:1303.4571 [hep-ex].
- [2] G. Aad *et al.* [ATLAS Collaboration], Phys. Lett. B **716**, 1 (2012) [arXiv:1207.7214 [hep-ex]].
- [3] T. Aaltonen *et al.* [CDF and D0 Collaborations], Phys. Rev. Lett. **109**, 071804 (2012) [arXiv:1207.6436 [hep-ex]].
- [4] S.L. Glashow, Nucl. Phys. B **22** (1961) 579; S. Weinberg, Phys. Rev. Lett. **19** (1967) 19; A. Salam, in: Proceedings of the 8th Nobel Symposium, Editor N. Svartholm, Stockholm, 1968.
- [5] A. Djouadi, Phys. Rept. **457**, 1 (2008) [hep-ph/0503172].
- [6] CMS collaboration: CMS-PAS-HIG-13-005; (See also: Talk at the Moriond 2013 QCD session by Christophe Ochando).
- [7] ATLAS collaboration: ATLAS-CONF-2013-014; (See also: Talk at the Moriond 2013 EW session by Eleni Mountricha).
- [8] H. Nilles, Phys. Rept. **110** (1984) 1; H. Haber and G. Kane, Phys. Rept. **117** (1985) 75; R. Barbieri, Riv. Nuovo Cim. **11** (1988) 1; J. D. Lykken, hep-th/9612114; J. Wess and J. Bagger, *Supersymmetry and Supergravity*, 2nd ed., (Princeton, 1991); D. J. H. Chung, L. L. Everett, G. L. Kane, S. F. King, J. D. Lykken and L. T. Wang, Phys. Rept. **407**, 1 (2005); M. Drees, P. Roy and R. M. Godbole, *Theory and Phenomenology of Sparticles*, (World Scientific, Singapore, 2005); H. Baer and X. Tata, *Weak scale supersymmetry: From superfields to scattering events*, Cambridge, UK: Univ. Pr. (2006) 537 p.
- [9] A. Djouadi, Phys. Rept. **459**, 1 (2008) [hep-ph/0503173].
- [10] S. P. Martin, arXiv:hep-ph/9709356; S. Heinemeyer, Int. J. Mod. Phys. A **21** (2006) 2659 [arXiv:hep-ph/0407244].
- [11] S. Heinemeyer, W. Hollik and G. Weiglein, Phys. Rept. **425** (2006) 265 [arXiv:hep-ph/0412214].
- [12] A. Arbey, M. Battaglia, A. Djouadi, F. Mahmoudi and J. Quevillon, Phys. Lett. B **708**, 162 (2012) [arXiv:1112.3028 [hep-ph]]; P. Draper, P. Meade, M. Reece and D. Shih, Phys. Rev. D **85**, 095007 (2012) [arXiv:1112.3068 [hep-ph]]; S. Akula, B. Altunkaynak, D. Feldman, P. Nath and G. Peim, Phys. Rev. D **85**, 075001 (2012) [arXiv:1112.3645 [hep-ph]]; M. Carena,

- S. Gori, N. R. Shah and C. E. M. Wagner, *JHEP* **1203**, 014 (2012) [arXiv:1112.3336 [hep-ph]]; A. Arbey, M. Battaglia and F. Mahmoudi, *Eur. Phys. J. C* **72**, 1906 (2012) [arXiv:1112.3032 [hep-ph]]; J. -J. Cao, Z. -X. Heng, J. M. Yang, Y. -M. Zhang and J. -Y. Zhu, *JHEP* **1203**, 086 (2012) [arXiv:1202.5821 [hep-ph]]; M. Carena, S. Gori, N. R. Shah, C. E. M. Wagner and L. -T. Wang, *JHEP* **1207**, 175 (2012) [arXiv:1205.5842 [hep-ph]]; M. Carena, I. Low and C. E. M. Wagner, *JHEP* **1208**, 060 (2012) [arXiv:1206.1082 [hep-ph]]; M. Carena, S. Gori, I. Low, N. R. Shah and C. E. M. Wagner, *JHEP* **1302**, 114 (2013) [arXiv:1211.6136 [hep-ph]]; A. Chakraborty, B. Das, J. L. Diaz-Cruz, D. K. Ghosh, S. Moretti and P. Poulose, arXiv:1301.2745 [hep-ph]; M. Carena, S. Heinemeyer, O. Stl, C. E. M. Wagner and G. Weiglein, arXiv:1302.7033 [hep-ph].
- [13] M. Carena, S. Gori, N. R. Shah, C. E. M. Wagner and L. -T. Wang, arXiv:1303.4414 [hep-ph].
- [14] A. Djouadi and J. Quevillon, arXiv:1304.1787 [hep-ph].
- [15] S. Heinemeyer, O. Stal and G. Weiglein, *Phys. Lett. B* **710**, 201 (2012) [arXiv:1112.3026 [hep-ph]].
- [16] R. Benbrik, M. Gomez Bock, S. Heinemeyer, O. Stal, G. Weiglein and L. Zeune, *Eur. Phys. J. C* **72**, 2171 (2012) [arXiv:1207.1096 [hep-ph]]; J. Ke, H. Luo, M. -x. Luo, K. Wang, L. Wang and G. Zhu, arXiv:1211.2427 [hep-ph]; J. Chang, K. Cheung, P. -Y. Tseng and T. -C. Yuan, *Phys. Rev. D* **87**, 035008 (2013) [arXiv:1211.3849 [hep-ph]]; J. Ke, H. Luo, M. -x. Luo, T. -y. Shen, K. Wang, L. Wang and G. Zhu, arXiv:1212.6311 [hep-ph]; A. Arbey, M. Battaglia and F. Mahmoudi, arXiv:1303.7450 [hep-ph].
- [17] P. Bechtle, S. Heinemeyer, O. Stal, T. Stefaniak, G. Weiglein and L. Zeune, arXiv:1211.1955 [hep-ph].
- [18] K. Hagiwara, J. S. Lee and J. Nakamura, *JHEP* **1210**, 002 (2012) [arXiv:1207.0802 [hep-ph]].
- [19] R. Barate *et al.* [LEP Working Group for Higgs boson searches and ALEPH and DELPHI and L3 and OPAL Collaborations], *Phys. Lett. B* **565**, 61 (2003) [hep-ex/0306033].
- [20] M. Drees, *Phys. Rev. D* **71**, 115006 (2005) [hep-ph/0502075].
- [21] M. Drees, *Phys. Rev. D* **86**, 115018 (2012) [arXiv:1210.6507 [hep-ph]].
- [22] N. D. Christensen, T. Han and S. Su, *Phys. Rev. D* **85**, 115018 (2012) [arXiv:1203.3207 [hep-ph]]; M. Asano, S. Matsumoto, M. Senami and H. Sugiyama, *Phys. Rev. D* **86**, 015020 (2012) [arXiv:1202.6318 [hep-ph]].

- [23] N. D. Christensen, T. Han and T. Li, Phys. Rev. D **86**, 074003 (2012) [arXiv:1206.5816 [hep-ph]].
- [24] U. Ellwanger, C. Hugonie and A. M. Teixeira, Phys. Rept. **496** (2010) 1 [arXiv:0910.1785]; M. Maniatis, Int. J. Mod. Phys. A **25**, 3505 (2010) [arXiv:0906.0777].
- [25] G. Belanger, U. Ellwanger, J. F. Gunion, Y. Jiang, S. Kraml and J. H. Schwarz, JHEP **1301**, 069 (2013) [arXiv:1210.1976 [hep-ph]];
- [26] D. G. Cerdeno, P. Ghosh and C. B. Park, arXiv:1301.1325 [hep-ph].
- [27] J. F. Gunion, Y. Jiang and S. Kraml, Phys. Rev. D **86**, 071702 (2012) [arXiv:1207.1545 [hep-ph]].
- [28] G. Belanger, U. Ellwanger, J. F. Gunion, Y. Jiang and S. Kraml, arXiv:1208.4952 [hep-ph].
- [29] [CMS Collaboration], Note CMS PAS HIG-2012-050.
- [30] [ATLAS Collaboration], Note ATLAS-CONF-2012-160.
- [31] A. Arbey, M. Battaglia, A. Djouadi and F. Mahmoudi, Phys. Lett. B **720**, 153 (2013) [arXiv:1211.4004].
- [32] [CMS Collaboration], CMS-PAS-HIG-11-029.
- [33] G. Aad *et al.* [ATLAS Collaboration], JHEP **1206**, 039 (2012) [arXiv:1204.2760 [hep-ex]].
- [34] S. Schael *et al.* [ALEPH and DELPHI and L3 and OPAL and LEP Working Group for Higgs Boson Searches Collaborations], Eur. Phys. J. C **47**, 547 (2006) [hep-ex/0602042].
- [35] R. Aaij *et al.* [LHCb Collaboration], Phys. Rev. Lett. **110**, 021801 (2013) arXiv:1211.2674.
- [36] S. R. Choudhury and N. Gaur, Phys. Lett. B **451**, 86 (1999); K. S. Babu and C. Kolda, Phys. Rev. Lett. **84**, 228 (2000); A. Dedes, H. K. Dreiner, and U. Nierste Phys. Rev. Lett. **87**, 251804 (2001); P. H. Chankowski and L. Slawianowska, Phys. Rev. D **63**, 054012 (2001) [hep-ph/0008046]; R. Arnowitt, B. Dutta, T. Kamon and M. Tanaka, Phys. Lett. B **538** (2002) 121; J. K. Mizukoshi, X. Tata and Y. Wang, Phys. Rev. D **66**, 115003 (2002); S. Baek, P. Ko, and W. Y. Song, JHEP **0303**, 054 (2003); G. L. Kane, C. Kolda and J. E. Lennon, hep-ph/0310042; T. Ibrahim and P. Nath, Phys. Rev. D **67**, 016005 (2003); J.R. Ellis, K.A. Olive and V.C. Spanos, Phys. Lett. B **624**, 47 (2005); S. Akula, D. Feldman, P. Nath and G. Peim, Phys. Rev. D **84**, 115011 (2011) [arXiv:1107.3535 ]; A. J. Buras, J. Girrbach, D. Guadagnoli and G. Isidori, arXiv:1208.0934.



- [37] Y. Amhis *et al.* [Heavy Flavor Averaging Group Collaboration], arXiv:1207.1158 [hep-ex].
- [38] G. Isidori and P. Paradisi, Phys. Lett. B **639**, 499 (2006) [hep-ph/0605012]; B. Bhattacharjee, A. Dighe, D. Ghosh and S. Raychaudhuri, Phys. Rev. D **83**, 094026 (2011) [arXiv:1012.1052].
- [39] J. P. Lees *et al.* [BABAR Collaboration], arXiv:1207.0698 [hep-ex].
- [40] G. Bertone, D. Hooper and J. Silk, Phys. Rept. **405**, 279 (2005) [hep-ph/0404175]; G. Jungman, M. Kamionkowski and K. Griest, Phys. Rept. **267**, 195 (1996) [hep-ph/9506380].
- [41] P. A. R. Ade *et al.* [Planck Collaboration], arXiv:1303.5076 [astro-ph.CO]; See also: G. Hinshaw *et al.* [WMAP Collaboration], arXiv:1212.5226 [astro-ph.CO].
- [42] E. Aprile *et al.* [XENON100 Collaboration], arXiv:1207.5988 [astro-ph.CO].
- [43] S. Bodenstein, C. A. Dominguez and K. Schilcher, Phys. Rev. D **85**, 014029 (2012) [arXiv:1106.0427]; G. -C. Cho, K. Hagiwara, Y. Matsumoto and D. Nomura, JHEP **1111**, 068 (2011) [arXiv:1104.1769 ]; D. Ghosh, M. Guchait, S. Raychaudhuri and D. Sengupta, Phys. Rev. D **86**, 055007 (2012) [arXiv:1205.2283 ]; S. Akula, P. Nath and G. Peim, Phys. Lett. B **717**, 188 (2012) arXiv:1207.1839.
- [44] H.E. Haber, R. Hempfling, A.H. Hoang, Z. Phys. **C75**, 539 (1997).
- [45] H.E. Haber and R. Hempfling, Phys. Rev. Lett. **66**, 1815 (1991); Y. Okada, M. Yamaguchi and T. Yanagida, Prog. Theor. Phys. **85**, 1 (1991), Phys. Lett. B **262**, 54 (1991); J. Ellis, G. Ridolfi and F. Zwirner, Phys. Lett. B **257**, 83 (1991), Phys. Lett. B **262**, 477 (1991).
- [46] W. Altmannshofer, M. Carena, N. R. Shah and F. Yu, JHEP **1301**, 160 (2013) [arXiv:1211.1976].
- [47] M. Liu and P. Nath, arXiv:1303.7472 [hep-ph]; J. Ellis and K. A. Olive, Eur. Phys. J. C **72**, 2005 (2012) [arXiv:1202.3262 ]; U. Chattopadhyay and D. Das, Phys. Rev. D **79**, 035007 (2009) [arXiv:0809.4065 ]; U. Chattopadhyay, D. Das, A. Datta and S. Poddar, Phys. Rev. D **76**, 055008 (2007) [arXiv:0705.0921 ]; U. Chattopadhyay, A. Corsetti and P. Nath, Phys. Rev. D **68**, 035005 (2003) [hep-ph/0303201].
- [48] A. Choudhury and A. Datta, arXiv:1305.0928 [hep-ph]; A. Choudhury and A. Datta, JHEP **1206**, 006 (2012) [arXiv:1203.4106 ]; N. Bhattacharyya, A. Choudhury and A. Datta, Phys. Rev. D **84**, 095006 (2011) [arXiv:1107.1997 ].
- [49] S. Alekhin, A. Djouadi and S. Moch, Phys. Lett. B **716**, 214 (2012) [arXiv:1207.0980 ].

- [50] J. Beringer *et al.* [Particle Data Group Collaboration], Phys. Rev. D **86**, 010001 (2012).
- [51] J. M. Frere, D. R. T. Jones and S. Raby, Nucl. Phys. B **222**, 11 (1983); J. A. Casas, A. Lleyda and C. Munoz, Nucl. Phys. B **471**, 3 (1996).
- [52] A. Arbey, M. Battaglia, A. Djouadi and F. Mahmoudi, JHEP **1209**, 107 (2012) [arXiv:1207.1348].
- [53] B. C. Allanach, A. Djouadi, J. L. Kneur, W. Porod and P. Slavich, JHEP **0409**, 044 (2004) [hep-ph/0406166].
- [54] G. Degrossi, S. Heinemeyer, W. Hollik, P. Slavich and G. Weiglein, Eur. Phys. J. C **28**, 133 (2003) [hep-ph/0212020].
- [55] R. V. Harlander, P. Kant, L. Mihaila and M. Steinhauser, Phys. Rev. Lett. **100**, 191602 (2008) [Phys. Rev. Lett. **101**, 039901 (2008)] [arXiv:0803.0672].  
S. P. Martin, Phys. Rev. D **75**, 055005 (2007) [hep-ph/0701051];
- [56] S. Bertolini, F. Borzumati and A. Masiero, Phys. Rev. Lett. **59**, 180 (1987); N. G. Deshpande, P. Lo, J. Trampetic, G. Eilam and P. Singer, Phys. Rev. Lett. **59**, 183 (1987); B. Grinstein and M. B. Wise, Phys. Lett. B **201**, 274 (1988); B. Grinstein, R. P. Springer and M. B. Wise, Phys. Lett. B **202**, 138 (1988); W. -S. Hou and R. S. Willey, Phys. Lett. B **202**, 591 (1988); B. Grinstein, R. P. Springer and M. B. Wise, Nucl. Phys. B **339**, 269 (1990).
- [57] S. Bertolini, F. Borzumati, A. Masiero and G. Ridolfi, Nucl. Phys. B **353**, 591 (1991); R. Barbieri and G. F. Giudice, Phys. Lett. B **309**, 86 (1993) [hep-ph/9303270]; R. Garisto and J. N. Ng, Phys. Lett. B **315**, 372 (1993) [hep-ph/9307301]; P. Nath and R. L. Arnowitt, Phys. Lett. B **336**, 395 (1994) [hep-ph/9406389]; M. Ciuchini, G. Degrossi, P. Gambino and G. F. Giudice, Nucl. Phys. B **534**, 3 (1998) [hep-ph/9806308].
- [58] M. S. Carena, D. Garcia, U. Nierste and C. E. M. Wagner, Phys. Lett. B **499**, 141 (2001) [hep-ph/0010003].
- [59] M. S. Carena, D. Garcia, U. Nierste and C. E. M. Wagner, Nucl. Phys. B **577**, 88 (2000) [hep-ph/9912516].
- [60] See Buras *et al.* of Ref. [36].
- [61] L. Roszkowski, S. Trojanowski, K. Turzynski and K. Jedamzik, arXiv:1212.5587.
- [62] I. Adachi *et al.* [Belle Collaboration], arXiv:1208.4678 [hep-ex].

- [63] M. Chakraborti, U. Chattopadhyay and R. M. Godbole, Phys. Rev. **D87**, 035022 (2013) arXiv:1211.1549.
- [64] M. Drees and M.M. Nojiri, Phys. Rev. D **48**, 3483 (1993) [hep-ph/9307208].
- [65] S. Akula and P. Nath, arXiv:1304.5526 [hep-ph]; S. Mohanty, S. Rao and D. P. Roy, J. High Energy Phys.11 (2012) 175 arXiv:1208.0894; M. A. Ajaib, T. Li and Q. Shafi, Phys. Rev. D **85**, 055021 (2012) [arXiv:1111.4467]; D. Das, A. Goudelis and Y. Mambrini, JCAP **1012**, 018 (2010) [arXiv:1007.4812]; D. Feldman, Z. Liu, P. Nath and B. D. Nelson, Phys. Rev. D **80**, 075001 (2009) [arXiv:0907.5392]; U. Chattopadhyay, D. Das, D. K. Ghosh and M. Maity, Phys. Rev. D **82**, 075013 (2010) [arXiv:1006.3045]; D. Feldman, Z. Liu and P. Nath, Phys. Rev. D **80**, 015007 (2009) [arXiv:0905.1148]; U. Chattopadhyay, D. Das and D. P. Roy, Phys. Rev. D **79**, 095013 (2009) [arXiv:0902.4568]; R. M. Godbole, M. Guchait and D. P. Roy, Phys. Rev. D **79**, 095015 (2009) [arXiv:0807.2390]; U. Chattopadhyay, D. Das, P. Konar and D. P. Roy, Phys. Rev. D **75**, 073014 (2007) [hep-ph/0610077]; G. Belanger, F. Boudjema, A. Cottrant, R. M. Godbole and A. Semenov, Phys. Lett. B **519**, 93 (2001) [hep-ph/0106275].
- [66] N. Fornengo, S. Scopel and A. Bottino, Phys. Rev. D **83**, 015001 (2011) [arXiv:1011.4743]; A. Bottino, F. Donato, N. Fornengo and S. Scopel, Phys. Rev. D **81**, 107302 (2010) [arXiv:0912.4025]; A. Bottino, V. de Alfaro, N. Fornengo, S. Mignola and S. Scopel, Astropart. Phys. **2**, 77 (1994) [hep-ph/9309219]; T. K. Gaisser, G. Steigman and S. Tilav, Phys. Rev. D **34**, 2206 (1986).
- [67] A. Djouadi, J. -L. Kneur and G. Moultaka, Comput. Phys. Commun. **176**, 426 (2007) [hep-ph/0211331].
- [68] G. Belanger, F. Boudjema, A. Pukhov and A. Semenov, Comput. Phys. Commun. **180**, 747 (2009) [arXiv:0803.2360]. Phys. Rev. D **34**, 2206 (1986).
- [69] G. Belanger, F. Boudjema, C. Hugonie, A. Pukhov and A. Semenov, JCAP **0509** (2005) 001 [arXiv:hep-ph/0505142].
- [70] G. Belanger, F. Boudjema, A. Pukhov and A. Semenov, Comput. Phys. Commun. **176**, 367 (2007) [arXiv:hep-ph/0607059].
- [71] A. Djouadi, M. M. Muhlleitner, M. Spira and , Acta Phys. Polon. B **38**, 635 (2007) [hep-ph/0609292].
- [72] J. Ellis and T. You, arXiv:1303.3879.

- [73] <https://indico.in2p3.fr/conferenceDisplay.py?confId=7411>
- [74] <http://moriond.in2p3.fr/QCD/2013/MorQCD13Prog.html>
- [75] CMS Collaborations: CMS-PAS-HIG-13-001, CMS-PAS-HIG-13-002, CMS-PAS-HIG-13-003, CMS-PAS-HIG-004, CMS-PAS-HIG-12-015.
- [76] ATLAS Collaborations: ATLAS-CONF-2013-012, ATLAS-CONF-2013-013, ATLAS-CONF-2013-030, ATLAS-CONF-2012-170.
- [77] T. Aaltonen *et al.* [CDF Collaboration], arXiv:1301.6668 [hep-ex]; V. M. Abazov *et al.* [D0 Collaboration], arXiv:1303.0823 [hep-ex].
- [78] E. Aprile [XENON1T Collaboration], arXiv:1206.6288 [astro-ph.IM].
- [79] U. Ellwanger, J. F. Gunion and C. Hugonie, JHEP **0502** (2005) 066 [arXiv:hep-ph/0406215].
- [80] U. Ellwanger and C. Hugonie, Comput. Phys. Commun. **175** (2006) 290 [arXiv:hep-ph/0508022].
- [81] T. Plehn, D. L. Rainwater and D. Zeppenfeld, Phys. Lett. B **454**, 297 (1999) [hep-ph/9902434].
- [82] D. Green, hep-ex/0501027.
- [83] J. M. Butterworth, A. R. Davison, M. Rubin and G. P. Salam, Phys. Rev. Lett. **100**, 242001 (2008) [arXiv:0802.2470].
- [84] Y. L. Dokshitzer, G. D. Leder, S. Moretti and B. R. Webber, JHEP **9708**, 001 (1997) [hep-ph/9707323].
- [85] ATLAS Public NOTE: ATL-PHYS-PUB-2009-088
- [86] T. Sjostrand, S. Mrenna and P.Z. Skands, JHEP **0605**, 026 (2006) arXiv:hep-ph/0603175.
- [87] M. Cacciari and G.P. Salam, Phys. Lett. **B641**, 57 (2006) arXiv:hep-ph/0512210; M. Cacciari, G.P. Salam and G. Soyez, arXiv:1111.6097.
- [88] <https://twiki.cern.ch/twiki/bin/view/LHCPhysics/CERNYellowReportPageAt14TeV>
- [89] T. Plehn, G. P. Salam and M. Spannowsky, Phys. Rev. Lett. **104**, 111801 (2010) [arXiv:0910.5472].

- [90] J. M. Butterworth, J. R. Ellis and A. R. Raklev, *JHEP* **0705**, 033 (2007) [hep-ph/0702150].
- [91] G. D. Kribs, A. Martin, T. S. Roy and M. Spannowsky, *Phys. Rev. D* **82**, 095012 (2010) [arXiv:1006.1656].
- [92] O. Stal and G. Weiglein, *JHEP* **1201**, 071 (2012) [arXiv:1108.0595].
- [93] B. Bhattacharjee, A. Chakraborty, D. Kumar Ghosh and S. Raychaudhuri, *Phys. Rev. D* **86**, 075012 (2012) [arXiv:1204.3369].
- [94] S. F. King, M. Muhlleitner, R. Nevzorov and K. Walz, *Nucl. Phys. B* **870**, 323 (2013) [arXiv:1211.5074].
- [95] Z. Kang, J. Li, T. Li, D. Liu and J. Shu, arXiv:1301.0453.
- [96] J. Alwall, M. Herquet, F. Maltoni, O. Mattelaer and T. Stelzer, *JHEP* **1106**, 128 (2011) [arXiv:1106.0522].